Investigation of Harmonine inhibition of NMDA receptors

Dennon-jay Brown Coker
1004949
Submitted for a Neuroscience Master of Research to the University of Nottingham
September 2022

Contents

Acknowledgements

I would like to thank my supervisors Dr Ian Mellor and Dr Paul Smith for all their guidance and support throughout my master's studies. I would also like to thank Liaque Latif and Maryam AL-NASSER who have trained me in DNA transformation, electrophysiological techniques, and gel electrophoresis. I'd like to thank the other students for which I did this project alongside, Abdul Rehman and Eleanor Johnson, for without this year would have been more difficult and much less enjoyable.

Abstract

N-methyl-D-aspartate receptors (NMDAR) is a critical ionotropic receptor in excitatory neurotransmission, it is a co-agonist receptor with a hetero tetrameric structure. It strengthens synaptic connections as it is involved in long term potentiation and is pivotal for learning and memory. GluN2A and GluN2B are crucial NMDAR subunits they differ in morphology and amino acids sequence which results in different Ca^{2+} currents, which are useful in different neural processes. NMDAR dysfunction can cause neurotoxicity, and this is seen in the Neurodegenerative disease, Alzheimer's disease (AD). The pathological hallmarks of AD, amyloid plaques interact with glutamate transporters in the tri-synapse. This pathway is one of many pathologies that lead to the cerebral atrophy seen in AD. Memantine is a FDA approved drug treatment for AD and used to treat moderate to severe symptoms. Research by Patel 2018 has shown that harmonine, an alkaloid produced by the harlequin ladybird, *Harmonia axyridis*, a key component of the organism's chemical defence can inhibit NMDAR activity. This inhibition makes harmonine a target for research as therapeutic treatment of AD. In this study the aim is to study the effects of harmonine on human NMDAR clones. Two-electrode voltage clamp was used to examine the effects of memantine and harmonine in a concentration dependent manner, in Xenopus oocytes expressing the NMDAR clones. The IC_{50} values revealed that harmonine blocks NMDAR in a concentration-dependent manner and is more potent than memantine at a membrane potential of -75 mV.

1 Introduction

1.1 NMDAR

Receptors are ubiquitous in organic biological systems and immensely important as their downstream effects include cell growth, death, division, and the opening of membrane channels. The binding of ligand causes a conformational change in the protein structure leading to these effects. A receptor of key significance in excitatory transmission is the N-Methyl D-Aspartate receptor (NMDAR), an ionotropic glutamate receptor (iGluR). iGluRs primarily bind glutamate and in response open their ion channel to allow for the rapid depolarisation of the membrane. The iGluR family consists of four subtypes in vertebrates: α-amino-3-hydroxy-5-methyl-4-isoaxazolepropionic acid (AMPA), kainate (KA), N-methyl-d-aspartate (NMDA), and δ-receptors (Twomey and Sobolevsky, 2017). This family of receptors shares many features such predominate co-localisation on the postsynaptic membrane and their modular structure (Regan, Romero-Hernandez and Furukawa, 2015). An extracellular domain (ECD) comprised of the amino-terminal domain (ATD) and ligand binding domain (LBD), the transmembrane domain (TMD) and carboxy-terminal domain (CTD) (Wollmuth and Sobolevsky, 2004; Traynelis et al., 2010). At the postsynaptic terminal the early phase of a excitatory post-synaptic potential (EPSP) is due to non-NMDARs while NMDARs contribute to the late phase of the EPSP (Regan, Romero-Hernandez and Furukawa, 2015).

NMDA is a co-agonist receptor subclass, that requires the binding of glutamate and glycine/D-serine for its activation and opening of its pore (removal of the Mg^{2+} block)(Mayer, Westbrook and Guthrie, 1984; Le Bail *et al.*, 2014). This causes an influx of Ca^{2+} and subsequently an increase in intracellular $[Ca^{2+}]$ ($[Ca^{2+}]_i$) (Mayer, Westbrook and Guthrie, 1984). A key characteristic of NMDARs is that they possess a Mg^{2+} block that occupies the pore at the resting membrane potential (-70 mV) even when the agonists are bound the receptor. The NMDAR Mg^{2+} block is voltage-dependent, so depolarisation of the membrane relieves the Mg^{2+} block allowing ion transportation (Burnashev et al., 1992). Just like the other iGluRs NMDARs are permeable to Na^+, K^+ and Ca^{2+}, its permeability to Na^+ and K^+ are low but it has the highest permeability to Ca^{2+} amongst all the iGluRs. This property allows NMDARs to initiate synaptic plasticity as Ca^{2+} acts a secondary messenger in this process (Lynch et al., 1983).

NMDARs are expressed at many different stages of an organism's life and have a critical role in learning, memory, and synaptogenesis (LYNCH, 2004; Traynelis et al., 2010). NMDARs are heterotetramers described as Hebbian-like coincidence detectors, as the opening of the pore requires the binding of glutamate and glycine/D-serine, along with depolarisation of the membrane to relieve the Mg^{2+} block (Retchless, Gao and Johnson, 2012). This creates

the association between the presynaptic release of glutamate and postsynaptic depolarisation (Collingridge and Bliss, 1987).

NMDARs are encoded by the gene families GRIN1, GRIN2 and GRIN3. GRIN1 encodes the GluN1 subunit which can be expressed as eight splice variants, GluN1-1a to GluN1-4a and GluN1-1b to GluN1-4b (Vance, Hansen and Traynelis, 2012). The “a” and “b” refer to the exclusion or inclusion of a 21 amino-acid residue located on exon 5, the inclusion of this exon has an effect on deactivation, open probability and agonist potency of the NMDAR (Vance, Hansen and Traynelis, 2012). The GRIN2 family possesses 4 genes GRIN2A (GluN2A), GRIN2B (GluN2A), GRIN2C (GluN2C) and GRIN2D (GluN2D), these variants result in differences in the amplitude of NMDAR potential, deactivation, and open probability (Yuan et al., 2009). GRIN3 has the variants GRIN3A (GluN3A) and GRIN3B (GluN3B), these variations show differences in their resistance to channel blockers (McClymont, Harris and Mellor, 2012). The wide variety of subunit combinations and their diversity in kinetics and physiological hints at critical role for NMDARs.

1.1.1 NMDAR Structure and function

Typically, NMDAR are comprised of two GluN1 subunits and two GluN2 subunits. GluN1 subunits bind the agonist glycine to the LBD, and GluN2 subunits bind glutamate to its LBD (Karakas and Furukawa, 2014). The combination of these four subunits predominantly forms a heterotetramer formed by two hetero dimers e.g., GluN1A – GluN2B + GluN1A – GluN2B, so effectively NMDARs are dimers of dimers. NMDAR subunits contain two extracellular domains ATD (formed by the R1 and R2 lobes) and LBD (formed by two discontinuous segments (S1 and S2), a TMD comprised of three transmembrane regions (M1, M3 AND M4), a re-entrant loop (M2/pore-loop) (figure 1.1.1.2) and pore-lining region and intracellular CTD (figure 1.1.1.1) (Retchless, Gao and Johnson, 2012; Lee et al., 2014; Liu et al., 2019).

These modular structures interact with each other via linkers between the domains, these linkers allow for the translation of certain conformational changes of one domain to than affect the following domain in an almost cascade like manner (Esmenjaud et al., 2018). Some of these features lead to structural constraints causing a degree of homogeneity amongst NMDAR, one such example is the organisation of the dimers and why they are heterodimers and not homodimers. The arrangement of these subunits that is favoured is heterodimers (1-2-1-2) not homodimers (1-1-2-2), this is due to collisions in the LDB when in the 1-1-2-2 combination. GluN1A-GluN1A is prevented by the collision of loop 1 of one subunit and helix G of the other, whereas GluN2B-GluN2B causes a structural hinderance between helix K’ of one subunit and helices E’ and F’ of the other (Karakas and Furukawa, 2014).

The most distal extracellular domain from the membrane of NMDARs is the ATD. The ATD is composed of the first ~350 amino acids of the subunit protein and forms clamshell-like structures from the R1 and R2 lobes, this domain is the interaction site for many allosteric modulators such as zinc and ifenprodil (figure 1.1.1.3) (Paoletti, Ascher and Neyton, 1997; Yuan et al., 2009). Many residues in the ATD have been proven to affect the affinity of allosteric molecules to NMDARs. H42, H44, H128, K233, and E266 are few of the residues discovered to be a critical for zinc inhibition of GluN2A subunits (Choi and Lipton, 1999; Fayyazuddin et al., 2000). Yuan et al., 2009 through a series of experiments found that the ATD affects the deactivation time of GluN2 subunits through the removal of ATD, and that it affects the subunit in different ways depending on the variant. It either slows the deactivation time or accelerates it. ATD affects agonist potency, deactivation time and open probability (P_{OPEN}) (Gielen et al., 2009; Yuan et al., 2009). As mentioned before linkers between domains are able to transmit the conformational changes of one domain to another. The covalent links of the R2 lobe of the ATD are able to transmit allosteric signals to the LBD (Lee et al., 2014). These linkers have extended and compact conformations depending on subunit dimer they are present in (Gielen et al., 2009; Yuan et al., 2009).

The LBD like the ATD has a clamshell-like structure comprised of the S1 and S2 segments, and as the name suggests they are the binding site of the agonist. Binding of the agonist to the LBD causes a large conformational change involving the closure of the clamshell-like structure, this movement is required for opening of the ion channel (Armstrong et al., 1998). This closed clamshell structure is stabilised through hydrogen bonds by a group of amino acids (Kalbaugh, VanDongen and VanDongen, 2004). There are molecular dynamic simulations of the NMDAR LBD that suggest many different conformations of the protein, a wide energy landscape was predicted, meaning these conformations are weakly stable and can change (Dai and Zhou, 2013; Yao et al., 2013). The two LBD of the tetramer will rotate to go from an inactive state to an active state which opens the channel, but this also depends on the conformation of the ATD (Gielen et al., 2008; Tajima et al., 2016). This rotation/rolling motion is key for NMDAR activation as the motion exerts force through the LBD-TMD linkers that pull the channel open (Esmenjaud et al., 2018)

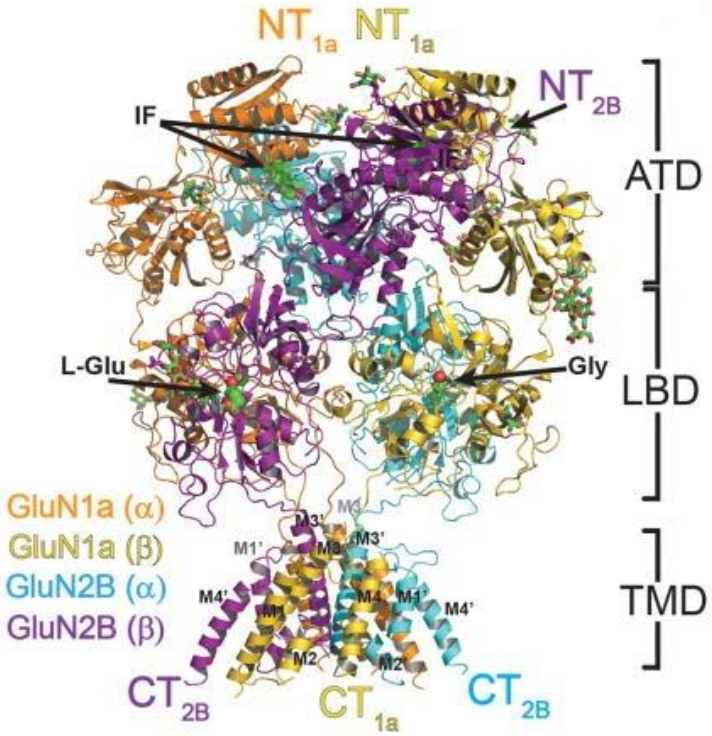

Figure 1.1.1.1: The crystal structure of heterotetrameric GluN1A-GluN2B NMDAR. The overall structure of the GluN1A-GluN2B receptor has been labelled to show the ATD, LBD and TMD. The heterodimers GluN1A (α) - GluN2B (α) and GluN1A (β) - GluN2B (β) have formed the tetramer. Agonists L-glutamate (L-Glu) and glycine (Gly) represented by green spheres are bound to the clamshell/bi-lobed structures in LBD, L-Glu bound to GluN2B and Gly bound to GluN1A. Ifenprodil, a negative allosteric modulator is bound to ATD of both GluN2B subunits (Karakas and Furukawa, 2014).

The TMD (figure 1.1.1.2) is comprised of M1, M3, M4 and the re-entrant pore loop (M2) between the M1 and M3 helices which forms the selectivity filter (Traynelis et al., 2010). The itself pore contains an asparagine residue that determines Ca^{2+} permeability and the Mg^{2+} block. There is a single residue that varies between GluN2 subunits that is responsible for channel properties observed between theses subunits (Glasgow, Siegler Retchless and Johnson, 2014). The influence of this site on channel properties also relies on its interaction with the GluN1 pore-loop, some subunit-subunit/dimer-dimer interactions are crucial for determining channel properties (Glasgow, Siegler Retchless and Johnson, 2014). One of the main forces that alter the channels state is the ATD-LBD, these two domains are tightly

bound together through linkers more so than other iGluRs, predominately these two act as single domain to modulate the P_{OPEN} of the receptor (Karakas and Furukawa, 2014).

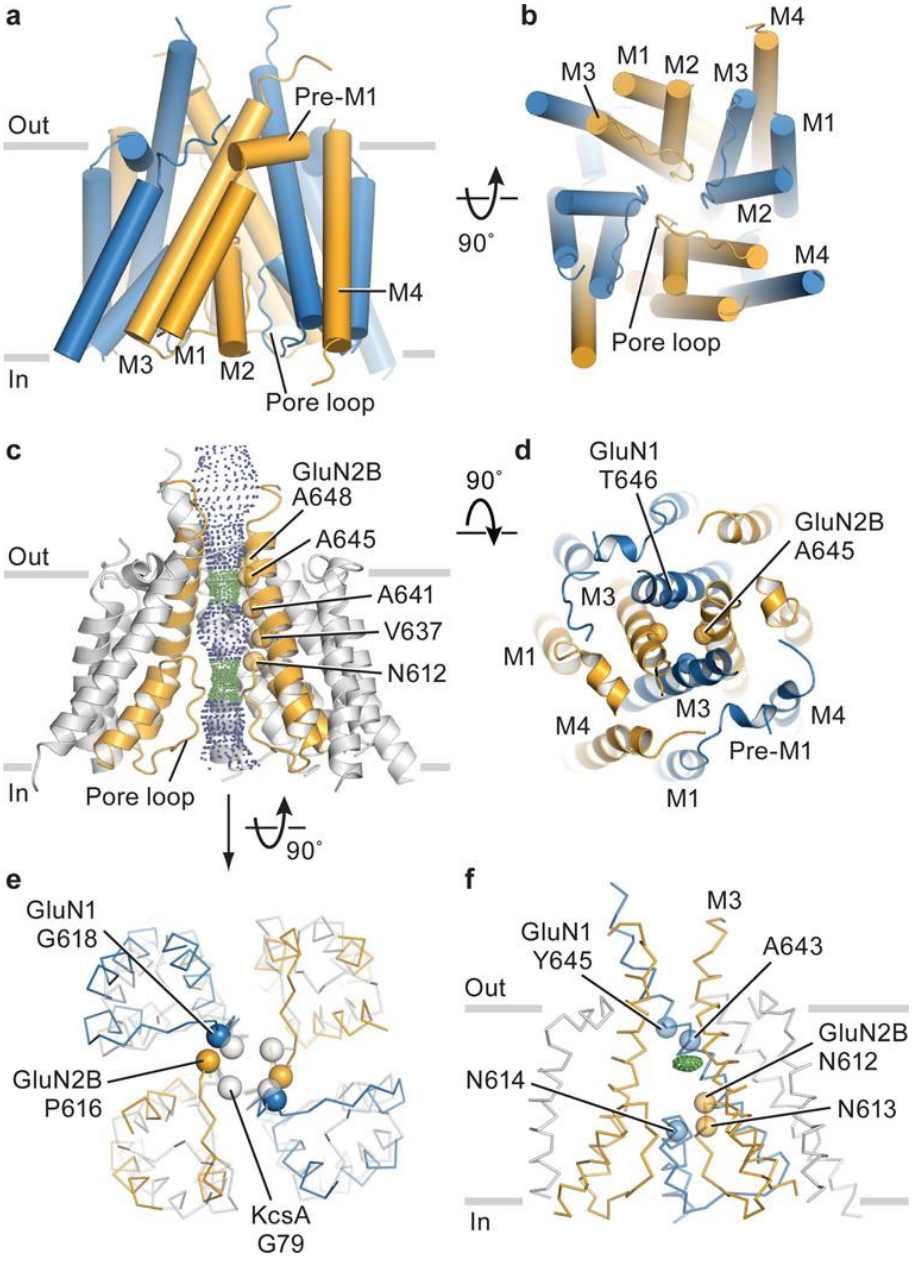

Figure 1.1.1.2: TMD architecture of a GluN1A-GluN2B NMDAR. (a) a parallel view of the TMD, GluN1A (blue) GluN2B (yellow). (b) the view of the TMD pore from the intracellular region looking outwards to the extracellular matrix. (c) a parallel view of the TMD showing the approximate size of the pore and the pathway from extracellular matrix, through the pore to intracellular matrix. Green dots represent a radius of 0.115 – 0.23 nm, and blue dots represent a radius greater than 0.23 nm. (d) a view of the M3 helices from the extracellular side. The spheres represent atoms of the Thr 646 and Ala 645 of the GluN1A-GluN2B. (e) a view of the TMD from the intracellular side with the image superimposed onto a K^+ channel.

(f) a parallel view of the TMD showing a positive electron density (green object) (Lee et al., 2014).

As stated above the opening of NMDARs requires the binding of glutamate, glycine, membrane depolarisation and the relief of the Mg^{2+} block from the pore, the resulting Ca^{2+} influx triggers the signal pathway for synaptic plasticity. In a physiological scenario strong and prolonged presynaptic release of glutamate activates AMPA receptors, this then causes the subsequent depolarisation of membrane and removal of Mg^{2+} from NMDAR pore (Liu et al.,2019). The signal pathway that results from Ca^{2+} influx is mediated by the intracellular CTD associates with proteins in the postsynaptic density which initiate intracellular signalling cascades critical for synaptic plasticity (Karakas and Furukawa, 2014).

In the synapse NMDARs are expressed in three locations, the presynaptic terminal where they can regulate glutamate release and mould synaptic plasticity by inducing BDNF via Ca^{2+} signalling (Park, Popescu and Poo, 2014). At the synapse where they form a large macromolecular NMDAR complex at the PSD, this complex contains scaffolding, adaptor and effector proteins that contribute to signalling cascades, NMDAR function and protein trafficking (Sheng and Lee, 2000). Extrasynaptic NMDARs are localised on dendritic shaft, spine neck or soma (Newpher and Ehlers, 2008). Some of the differences between synaptic and extrasynaptic localised NMDARs are, GluN2A receptors are preferentially included in synaptic NMDARs and GluN2B subunits in extrasynaptic NMDARs (Groc et al., 2006; Papouin et al., 2012). Another characteristic is that glutamate concentration is higher at the synapse compared to extrasynaptic localisation, the last one is the duration of glutamate exposure, extrasynaptic NMDARs are exposed to glutamate for longer periods of time compared to synaptic NMDARs (Glasgow et al., 2017). NMDARs are critical for synaptic plasticity but the requirements for long-term potentiation (LTP) and long-term depression (LTD) are different. Synaptic NMDAR activation and large increases in $[Ca^{2+}]_I$ are needed for LTP. The large increase in $[Ca^{2+}]_I$ triggers a Ca2+/calmodulin-dependent protein kinase II (CaMKII)-mediated signalling cascade that leads to an enhanced synaptic strength by via recruitment of iGluRs (Liu et al., 2019a). LTD requires activation of extrasynaptic NMDAR, endocytosis of synaptic NMDAR and lower increases in $[Ca^{2+}]_i$ are required for LTD (Liu et al., 2019a).

NMDARs are expressed in a wide variety of non-neuronal cells e.g., in bones, kidneys and the pancreas (Hogan-Cann and Anderson, 2016). In the central nervous system (CNS), NMDARs are a key contributor to healthy and neurotypical physiology, so disease states of NMDAR can have quite debilitating effects. Hypofunction can result in impairment and hyperfunction can result in neurotoxicity. Experiments using null mutants of GluN1A-GluN2A receptors demonstrated that NMDAR hypofunction can result in impaired LTP induction in postsynaptic mossy fibres and cerebellar dependent learning (Andreescu et al.,

2011). NMDAR hypofunction is also associated with schizophrenia and memory impairment which can be induced from relatively low doses of NMDAR antagonists (Traynelis et al., 2010).

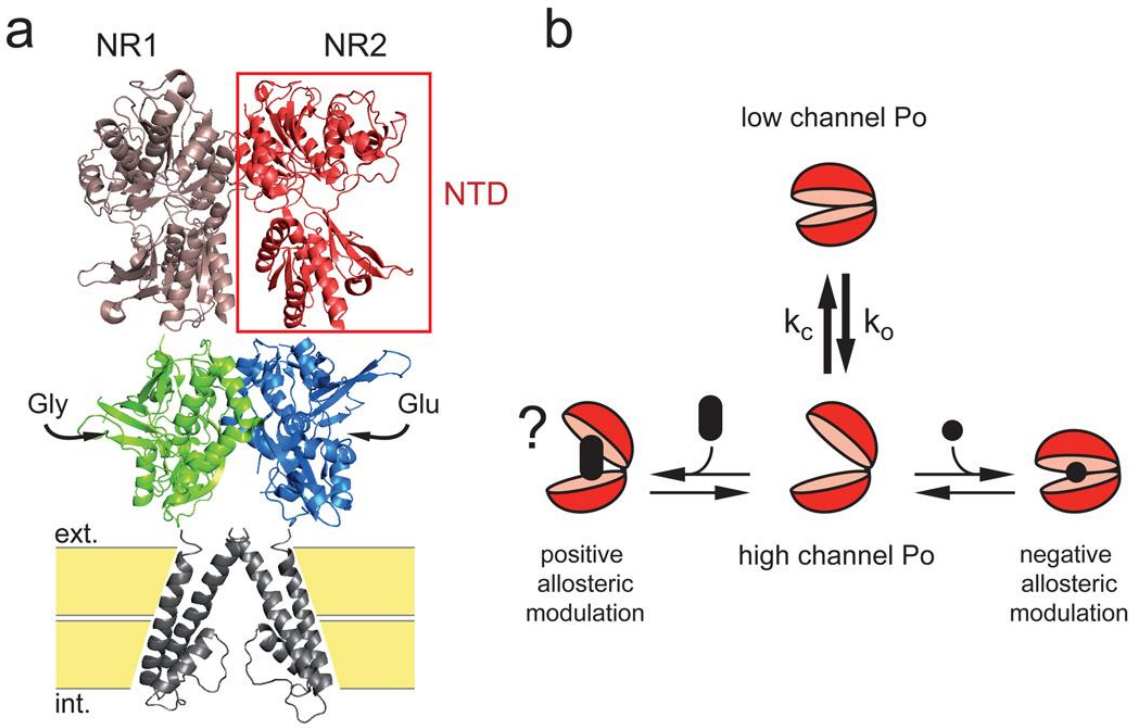

Figure 1.1.1.3 The modulation of NMDAR activity by the NR2 NTD/ATD. (a) The structural depiction of a NR1/NR2 receptor but only the NR1 and NR2 are shown in their respective heterodimer. (b) Visualisation of the clamshell structure of the NR2-NTD in its ligand-free state alternating between an open and closed-cleft conformation, with the latter favouring pore closure. Binding of negative allosteric modulators such as ifenprodil and zinc bind to the NR2. The action of a positive allosteric modulator preventing closure (Gielen et al., 2009).

1.2 Alzheimer's Disease

Neurodegenerative diseases affect millions of people worldwide especially the elderly. Such diseases are rapidly prevalent and are happening on a global scale in both developed and developing nations. Such diseases are more prevalent with age and are a threat to our aging population (Qiu, Kivipelto and Strauss, 2009) Dementia is the most common neurodegenerative disease and characterised as the severe decline cognitive ability. 60 – 80% of dementia cases are Alzheimer's disease (AD) (Alzheimer's Association, 2019). Approximately 40 million people worldwide are suffering from AD and the number of patients doubles every 20 years (Liu et al., 2019b). AD pathology has key pathological

markers such as extracellular amyloid-beta (Aβ) plaques, intracellular aggregates of phosphorylated tau protein, loss of cerebral tissue (Qiu, Kivipelto and Strauss, 2009). There are two types of AD familial and sporadic, familial is mostly genetic and has big correlation with family history of the disease. Some of genes involved in familial AD are Presenilin-1 and Presenilin-2. These two genes are involved the processing of the amyloid precursor protein (APP) incorrect cleaving of APP is what leads to the production of a 42-sequence Aβ variant that is aggregate in intracellular and extracellular matrix and disrupt cell function (Bi et al., 2002).

Increased $A\beta_{42}$ peptide causes NMDAR-dependent synaptic depression and spine elimination, hence affecting the glutamatergic system (Liu et al., 2019a). This is not the only system AD is involved in as it is a multifactorial disease with several processes making up its aetiology e.g., NMDA (glutamatergic), cholinergic, Aβ and tau. (Liu et al., 2019b). Disruption of the glutamatergic system happens via exotoxicity through excessive Ca^{2+} signalling, this excess is theorised to happen through extrasynaptic NMDAR and this correlates as those are the receptors predominately involved in LTD (Wang and Reddy, 2017). This excess of glutamate activity at the receptors is due to reduced glutamate reuptake (Fernández-Tomé et al., 2004). This reduced reuptake can happen due to extra-cellular aggregates of $A\beta_{42}$ blocking glutamate transporters leading to excess glutamate in the receptor region.

1.3 Memantine

Memantine is an FDA-approved drug and is the only current treatment for moderate to severe AD patients. It is an open channel blocker and binds to the pore of NMDAR in a voltage-dependent manner (Blanpied et al., 1997; Gilling et al., 2009). Memantine has a low to moderate specificity to NMDAR and through Mini-Mental State Examination it was shown to have a significant but small improvement in neuropsychiatric symptoms, global functioning, cognition, and day to day living (Van Marum, 2009). A study by Dashniani et al., 2020 demonstrated that memantine can prevent impairment of hippocampal-dependent spatial memory caused by okadaic acid through NR2B and nicotinic acetylcholine receptor (nAChR) subunit expression.

Memantine has also been shown to have antagonistic effects on nAChRs, so its effects span both cholinergic and glutamatergic pathways, and is essentially a multi-ligand drug treatment (Lee et al., 2012).

1.4 Harmonine

Harmonia axyridis (*H. axyridis*), is part of the Coleoptera order and within the lady beetle family *Coccinellidae*, from which there are roughly 6000 species (Seago et al., 2011). *H. axyridis* is also known as the Harlequin ladybird, native to subtropical parts of East and Central Asia. These ladybirds have been used as a biological control agent for aphids or pests for roughly a century, due to some of the survival mechanisms they have evolved (Röhrich et al., 2011). Originally, they were introduced as a biological control agent, then they became an invasive species. They have a diverse range of food sources, fungal resistance, and a microsporidian parasite lethal to native species but harmless to the harlequin (Yong, 2013). These factors can be contributed to the harlequin success as an invasive species and to outcompete native species. Contrary to the previous point, coccinellids have various natural enemies such as braconid wasps, crab spiders along with entomopathogenic nematodes and fungi (Nagel, 2016). To combat such threats the Harlequin ladybird feigns its death and releases haemolymph from the femorotibial joints of its legs, this fluid has deterrent and toxic properties that can affect the CNS. The toxic characteristic comes from the autogenous synthesised alkaloids present in the haemolymph (Daloze, Braekman and Pasteels, 1994). Alkaloids are natural organic compounds containing nitrogen, structured into a heterocyclic ring (Shields et al., 2008). These compounds are poorly soluble in water, but they will dissolve in solvents such as ether, chloroform, and methanol, which can be used to extract and separate these alkaloids.

Alkaloids are quite abundant and are present in clinical areas e.g. morphine, an anaesthetic, some have demonstrated antimalarial activity such as quinine and securinine (Peatey *et al.*, 2012; Vu *et al.*, 2013). Other well-known alkaloids include nicotine, caffeine, codeine and cocaine (Heinrich, Mah and Amirkia, 2021). These compounds are predominantly synthesised from amino acids and the ones currently in use are mainly derived from plants, with 20% of plant species producing alkaloids in small quantities (Srivastava and Srivastava, 2013; Heinrich, Mah and Amirkia, 2021). Harmonine ((17*R*,9*Z*)-1,17-diaminooctadec-9-ene), an insect-derived alkaloid is present in the haemolymph of *H. axyridis* and was identified as the key compound responsible for the haemolymph's antimicrobial properties (figure 1.4.1) (Röhrich et al., 2011). It may also be responsible for the lady bettles invasive success. Harmonine has shown to have application to the medical field as an anthelminthic specially schistosomiasis caused by the parasite *Schistosoma mansoni* (Kellershohn *et al.*, 2019). 5 µM of harmonine demonstrated antischistosomal activity *in vitro* and at a concentration 10 µM caused gonad dysplasia and halted egg production.

Another study conducted by Patel (2018) found that HAE, an extract from *H. axyridis* inhibits GluN1-1a/2a NMDAR at an IC_{50} of 0.179 µg/ml at Vh = -75 mV when expressed in *Xenopus* oocyte. HAE consists mostly of the compound harmonine (Figure 1.4.1).. Harmonine's inhibiting properties also extend to acetylcholinesterase (AChE), this is a notable target because decreased levels of acetylcholine (ACh) and loss of cholinergic neurons are a part of

AD pathology (Lane et al., 2005). This is emphasised by the fact that the current therapeutic treatment of AD is to inhibit AChE (Giacobini, 2004; Lane, Potkin and Enz, 2005).

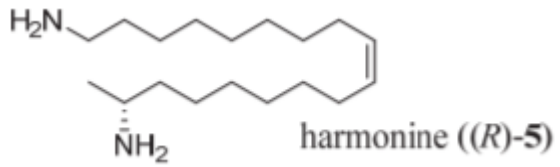

Figure 1.4.1: Structure of Harmonine ((17*R*,9*Z*)-1,17-diaminooctadec-9-ene) (Nagel, 2016).

The inhibition of GluN1A- GluN2A could help counter the neurotoxicity caused by NMDAR hyperfunction, and hence the neuronal cell death seen in neurodegenerative disorders. Currently, memantine is used as a treatment for AD as it is an NMDAR antagonist.

1.5 Aims and objectives

In this study the aim to study the effects of harmonine and its analogue on human NMDAR clones. Memantine as a clinically approved drug would provide comparison for harmonine to measure its therapeutic potential. Two-electrode voltage clamp was used to examine the effects of memantine and harmonine in a concentration dependent manner, in *Xenopus leavis* oocytes expressing the GluN1A-GluN2A and GluN1A-GluN2B clones. The potency, voltage-dependence and onset (tau) were measured and compared.

2 Methods and Materials

2.1 Materials

Table 2.1.1: List of reagents/chemicals used and their supplier.

Reagent	Supplier
Nuclease-free water	Sigma-Aldrich
Sodium Pyruvate	
HEPES, Free Acid	Corning
Agar Granulated	Melford
Tryptone enzymatic digest from casein	Fluka™
Yeast Extract	Sigma-Aldrich
Sodium Chloride (NaCl)	Fisher scientific
Agarose	Bioline
Gentamicin solution	Sigma-Aldrich
Collagenase from Clostridium	
Calcium chloride ($CaCl_2$)	Fluka™
Theophylline	Sigma-Aldrich
HEPES	
Dimethylsulphoxide (DMSO)	
Magnesium chloride ($MgCl_2$)	BDH Chemicals
Magnesium sulphide($MgSO_4$)	
D-Glucose anhydrous	Fisher scientific
Potassium Chloride (KCl)	Fluka™
Memantine HCL	ApexBio Tech LLC
Glycine	Sigma-Aldrich

N-Methyl-D-Asparate (NMDA)	Fisher Scientific
Ethidium bromide	Sigma-Aldrich
Ethylenediaminetetraacetic acid (EDTA)	
Ampicillin anhydrous	
Tris base	
Boric acid	
Sodium hydroxide (NaOH)	Fisher-Scientific
Hydrochloric acid (1M)	Sigma-Aldrich
dH_2O (minimum 11.8 MΩ)	-
Diethyl ether (HPLC grade)	Fisher-Scientific
Dichloromethane (HPLC grade)	
NotI (Restriction enzyme) rCutSmart buffer	Bio-Labs

2.2 Equipment

Table 2.2.1: Equipment used in the lab.

Equipment	**Supplier**
Eppendorf Centrifuge 5417 R	Eppendorf
P-97 Flaming/Brown	Sutter Instruments Co. US
N50 UV/Vis spectrophotometer	Implen ™
Nanoliter 2010 injector	World Precision Instruments (WPI)
HI 9321 Microprocessor pH meter	HANNA instruments

Table 2.2.2: Two-electrode Voltage Clamp equipment.

Equipment	Supplier
NI USB-6211 interface	National Instruments
GeneClamp 500B Amplifier	Axon Instruments
ValveLink^{TM} 8 (perfusion system interface)	AutoMate Scientific, Inc
HS-2A Headstage	Axon Instruments
Digidata 1200B-BNC Interface	Axon Instruments

2.3 Solutions used

The pH of all the solutions were adjusted using 2 M NaOH.

Table 2.3.1: Reagents used to make Xenopus ringer solution.

Xenopus Ringer	1 litre	dH_20	pH	7.5
	NaCl	**KCl**	**$CaCl_2$ (1M)**	**HEPES**
g/L	5.6	0.15	2	1.19
mM	95	2	2	5

Table 2.3.2: Reagents used for Barth's GTP. Gentamicin solution (10 mg/mL) was added at a concentration of 5ml/L after the solution was autoclaved.

Barth's GTP	1 litre	dH_20		pH	7.5
	NaCl	**KCl**	**$CaCl_2$ (1M)**	**HEPES**	**Sodium Pyruvate**	**Theophylline**
g/L	5.61	0.15	1.8	1.19	0.275	0.09
mM	96	2	1.8	5	2.5	0.5

Table 2.3.3: Reagents used for Luria-Bertani Broth.

Luria-Bertani Broth	1 litre	dH_20	pH	7.5
	NaCl	**Tryptone**	**Yeast extract**	
g/L	10	10	5	

Table 2.3.4: Reagents used for Luria-Bertani Broth Agar.

Luria-Bertani Broth Agar		1 litre	dH_20	pH	7.5
	NaCl	**Tryptone**	**Yeast extract**	**Agar**	
g/L	10	10	5	17	

Table 2.3.4: Reagents used for the stock solution of Tris-Boric EDTA.

5 x Tris-Boric-EDTA		1 litre	dH_20	pH	-
	Tris	**Boric acid**	**0.5M EDTA solution**		
g/L	54	27.5	20		

2.4 HAE Extraction

HAE is *Harmonia axyridis* alkaloid extract and is ~90% Harmonine.

Adult *Harmonia axyridis* beetles were captured from around the University Park campus of the University of Nottingham in the UK, where they were stored at -20°C. To extract the alkaloids, present in the haemolymph, methanol was used as a form of solvent extraction. The beetles were counted and transferred to a mortar where they were flash frozen with liquid nitrogen and then ground up.

2.4.1 Solvent Extraction

The first step of the extraction process is to add 50 ml of HPLC grade methanol to 100 beetles to create a 2 beetle/ml of HPLC methanol mixture, this mixture was then left to stir overnight at room temperature. The methanol was then decanted out and stored at 4°C. The previous step was then repeated with the same 100 beetles in 50 ml of methanol, and then methanol from both extractions was mixed together.

2.4.2 Acid-Base Extraction

The next step was an acid-base extraction which separates the alkaloids from the other compounds present in the methanol mixture. The methanol from the previous step was placed in a rotary evaporator until all of it had completely evaporated. The remaining precipitate/solid was washed with 2 ml of 1 M HCl and then transferred to a separation funnel. 50 ml of HPLC grade diethyl ether was used to wash the evaporator flask and the

contents were added to the separation funnel. The contents were then mixed, and the mixture was left till it formed two layers, an aqueous and an organic layer. The organic layer was discarded while the aqueous layer remained. This step was repeated twice, and the aqueous layers were all combined.

The collected aqueous layers were then adjusted to pH> 10 with 2 M NaOH and returned to the separation funnel. The glass wear used to adjust the pH was washed with 50 ml of HPLC dichloromethane (DCM) which was then added to the separation funnel. The funnel was mixed and left to separate into aqueous and organic layers, the layers were then decanted into separate vessels. The aqueous layer was returned to the funnel and this step was repeated, washing the aqueous layer vessel with 50 ml of DCM. All the separated organic layers were mixed and washed with 10 ml of saturated NaCl solution with 1 g of magnesium sulphate. This was then filtered with grade 4 filter paper. The remaining DCM was evaporated using the rotary evaporator, for the remaining precipitate it was dissolved with a minimal volume of DCM. The alkaloid extract was then evaporated by using pressurised nitrogen gas on the surface of the DCM. The precipitate was then weighed, ~ 1 mg of HAE is dissolved in 0.5 – 1 ml of DCM and aliquoted into glass ampoules sealed under nitrogen. The ampoules were then stored at 4°C.

2.5 Molecular Techniques

Human NMDAR pDNA clones were used in this study. GRIN1, GRIN2A and GRIN2B were purchased from GenScript Inc, the genes were inserted into pcDNA3.1+ /C-(K)-DYK vectors (GenEZ^{TM}) after the Kozak sequence. The vector contains other genes such as ampicillin resistance which is essential for the molecular biology techniques used. The clones arrive as 10 µg samples and they were centrifuged at 6,000 g for 1 minute at 4°C (Eppendorf centrifuge 5417 R, Eppendorf, Germany) then 100 µl of nuclease-free water was added for a stock concentration of 100 ng/µl. The vials were then stored at -20°C.

The first step of the transformation/transcription process was to select a subunit plasmid clone with ideally with a concentration of 100 – 200 ng/µL. If the concentration was too high (>400 ng/µL) it would be diluted to 150 - 200 ng/µL but the dilution was done at the end of the DNA transformation/mRNA transcription process.

2.5.1 DNA transformation

For each of the desired subunits being replicated, 2 µL of 2-Mercaptoethanol was added to 200 µL of XL10-Gold Ultracomponent *E.Coli* (sourced from Agilent Technologies, US) which

was left to rest for 10 minutes at room temperature. The solution was swirled every 2 minutes. Once 10 minutes had passed the solution was transferred to a new vessel and 2 µL of the desired pcDNA subunit (100 – 200 ng/µL) was added whilst making sure the tip was submerged in the bacteria solution. This was then left to rest on ice for 30 minutes while being swirled every 10 minutes. The solution was then transferred to a 42°C water bath for 45 seconds then back to the ice for 4 minutes, this heat shocks the bacteria. 950 µL of Super optimal catabolite repression medium (SOC) was added to the solution. SOC is made from LB with 10 mM of D-glucose and filtered through a 0.2 µm filter. The solution was then incubated at 37°C for 1 hour while being rotated at 250 rpm in a rotary incubator. The next step used Luria broth (LB) agar (refer to the solutions section), the agar had an ampicillin concentration of 50 µg/ml from a 100 mg/ml ampicillin salt solution diluted in dH_2O. A spreader is first sterilised using 100% ethanol and fire, and then 250 µL of the incubated bacteria solution is spread on an LB agar plate. The plate was then wrapped in parafilm and incubated overnight at 37°C (maximum time of 48 hours).

Once the incubation was complete the bacteria colonies in the petri dish can last for up to 1 month (wrap the dish with parafilm) then store at 4 – 8°C.

Bacteria colonies were scraped from the agar plates using a 200 µL pipette tip and placed in 5 mL of LB with an ampicillin concentration of 100 µg/mL. The fluid was then spun at 250 rpm, at 37°C overnight in a rotatory incubator.

2.5.2 DNA Isolation

Using the GenElute™ Plasmid Miniprep (70) Kit (SIGMA-Aldrich, US) the resuspension solution was prepared by centrifuging the RNA A solution to collect the solution at the bottom of the vessel. 78 µL of RNA A solution was added to the resuspension solution, mixed, and stored a 4°C. The wash solution was prepared beforehand by diluting the wash concentrate with 100 mL of 100% ethanol, mixed, and stored at room temperature.

The bacteria were harvested by transferring 1.5 mL of the recombinant bacteria solution into an Eppendorf tube and centrifuging it at >12000 rpm for 1 minute, the supernatant was then removed with a micropipette leaving only the pellet. This step was repeated until all of the recombinant bacteria had been harvested.

The remaining pellet was then resuspended in 200 µL of the aforementioned resuspension solution and mixed until the solution was homogenous. The bacteria were then broken down by adding 200 µL of the lysis solution, immediately followed by inverting the vessel 6 – 8 times. Once the solution is homogenous it should be transparent. The lysis reaction was left for 4 minutes and should not exceed 5 minutes, once 4 minutes had passed 350 µL of the neutralisation solution was added and the vessel was inverted 4 – 5 times. The solution was then centrifuged at 14000 rpm for 10 minutes.

A GenElute™ Miniprep column was prepared to maximise the binding of DNA to the membrane to increase the yield of DNA. The column was made by placing a miniprep column filter in a collection tube. 500 µL of column preparation solution was added to the collection tube and then centrifuged for 1 minute at 14000 rpm, the flow-through solution was then decanted. The lysate bacteria from the prior step was transferred to the ready-state column and centrifuged for 1 minute at 14000 rpm, the flow-through fluid was discarded. 750 µL of the wash solution was added to the column and centrifuged for 1 minute at 14000 rpm. The flow-through was discarded and the column was then centrifuged at the same speed for 2 minutes. This removes any excess ethanol from the membrane. To elute the DNA the column filter was placed in a new sterile collection tube then 50 µL of elution solution was added and centrifuged for 1 minute at 14000 rpm. The pDNA concentration was then measured using the Implen Nanophotometer™ (figure 1.5.2.1). 1 µL of elution solution was used as a blank for the machine, because the pDNA sample was diluted in elution solution. The equipment was set to dsDNA. A concentration above 150 ng/µL was desirable and an A26/280 (contamination) of 1.7 – 1.9.

Figure 2.5.2.1: The Implen NanoPhotometer™ N50 UV/Vis spectrophotometer for NanoVolume applications

2.5.3 DNA Restriction digest

Plasmid DNA was linearised to allow for mRNA transcription. The GRIN1A, GRIN2A and GRIN2B DNA samples were linearised using the restriction enzyme NotI. 1 µg of the desired DNA subunit was combined with 1 µl of NotI (Biolabs), the total volume was then made up to 50 µl with nuclease-free water in an Eppendorf. The reaction assembly was then mixed

and incubated at 37°C in a water bath for 2 hours. The reaction was terminated by adding 2.5 µl of a 0.5 M EDTA solution, and 5 µl of ammonium acetate (part of the mMESSAGE mMACHINE kit) with 150 µl of chilled, 100% ethanol. The mixture was then left overnight at -20°C.

The mixture was centrifuged at 4°C for 15 minutes at 14,000 g. The supernatant was decanted then centrifuged again at the maximum speed for 30 seconds, the supernatant was then decanted again. The vessel was placed with the lid open in a 50°C water bath for 5 minutes to dry the pellet. The DNA pellet was then resuspended in 5 µl of nuclease-free water. With the lid closed the mixture was incubated for 5 minutes in a 50°C water bath. The resuspension was centrifuged at maximum speed for 5 minutes. The concentration was measured with a spectrophotometer (figure 2.5.2.1).

2.5.4 Gel Electrophoresis

Gel electrophoresis confirms visually that pDNA has been linearised, and the restriction enzymes have cut the pDNA appropriately. A 0.5 M solution of EDTA was made and adjusted to a pH of 8 with a 2 M NaOH solution. 1xTris-Boric-EDTA (TBE) solution was made from 5xTBE stock solution by diluting 100 ml of the stock in 400 ml of dH_2O. 1 g agarose powder was added to 100 ml of the 1xTBE. The mixture was dissolved in the microwave in bursts to prevent boiling and any incidents such as the gel exploding in the microwave. 1 µl of 1 mg/ml ethidium bromide was added to the gel once the mixture had reached a temperature of ~40°C. The mixture was left to set in a mould, once it was ready it was moved to an electrophoresis tank (Bio-Rad). The gel was then submerged in 1xTBE, 1 µl of a 1 kb DNA ladder (Biolabs) (10 µl of the ladder with 2 µl of the loading dye) along with 1 µl of the DNA samples (1 µl DNA, 1 µl loading dye and 4 µl of nuclease-free water) were loaded into the wells. Linearised (cut) and circular (uncut) samples of GRIN1A and GRIN2A were loaded into the gel. The gel was run for 1 hour at 140 V (PowerPac 200, Bio-Rad) then the DNA bands were imaged on an iBright™ 750 (Invitrogen by Thermo Fisher Scientific). Figure 2.5.4.1 depicts an example of gels imaged.

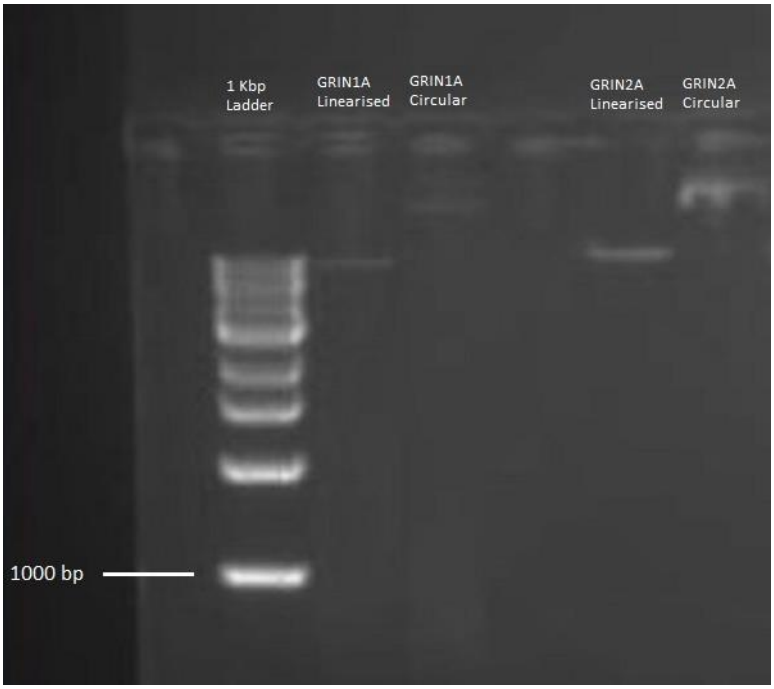

Figure 2.5.4.1: Gel image of DNA Samples. The image was taken on the iBright^{TM} 750 and depicts the bands of 1 kb DNA ladder, cut and uncut human pDNA clones of GRIN1A and GRIN2A. Both cut with NotI in separate reactions.

2.5.5 mRNA Transcription

Linearised DNA was transcribed into 5' end 7-methyl guanosine capped mRNA. For GRIN1A and GRIN2A the mMESSAGE mMACHINE SP6 promoter kit (Sigma-Aldrich) was used, and the T7 kit for GRIN2B. 3 µl of linearised DNA (50 – 200 ng/µL) was added to a 1.5 ml Eppendorf, 10 µl of 2 X NTP/CAP, 2 µl of 10 X enzyme mix, and 5 µl of nuclease-free water. The reaction assembly was mixed lightly with a pipette and then incubated for 2 hours at 37°C in a water bath. The RNA was recovered by adding 30 µl of lithium chloride precipitation solution and 30 µl of nuclease-free water. This mixture was then stored at -20°C overnight. The mixture was then centrifuged at 4°C at 24,000 for 30 minutes, afterwards, the supernatant was aspirated with a pipette. The RNA pellet was washed with 1 ml of 70% ethanol and centrifuged again for 30 minutes. The supernatant was decanted and centrifuged for 30 seconds; the Eppendorf was then placed with the lid open in a 50°C water bath for 5 minutes to dry the pellet. The pellet was then resuspended in 15 µl of nuclease-free water. The RNA concentration was then measured with the spectrophotometer before being stored at -80°C.

2.6 *Xenopus laevis* Oocyte expression

The *Xenopus laevis* (African clawed frog) oocytes were used to express the non-native NMDAR clones. Xenopus oocytes go through six stages of maturation (I – VI), and stages IV – V are used for electrophysiology studies. The oocytes were supplied by the European *Xenopus* Resource Centre, Portsmouth, UK, and Ecocyte Bioscience, Germany. The oocytes were removed from the ovaries of mature female African clawed frogs via ovariectomy. The oocytes were ~1 mm in diameter and have two visibly distinct regions, the nucleus containing animal pole and the vegetal pole (figure 2.6.0) (Bianchi and Driscoll, 2006).

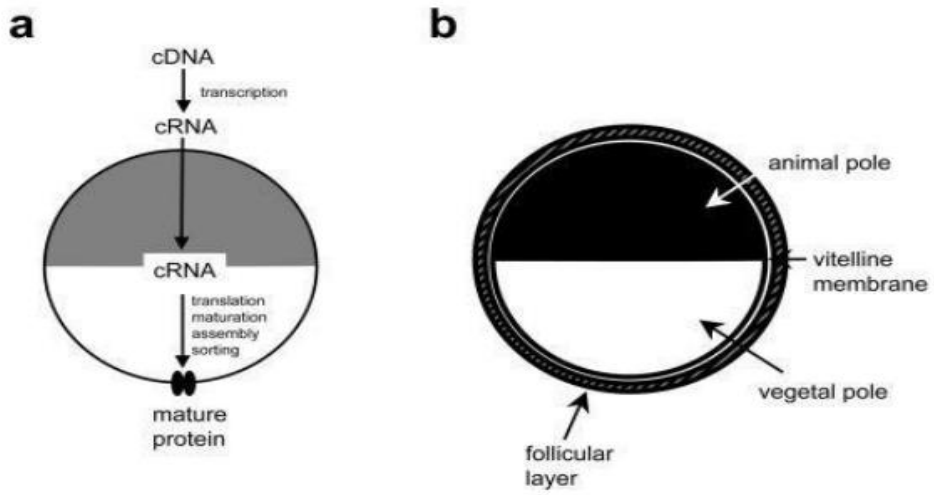

Figure 2.6.0: *Xenopus Oocytes.* A, this diagram represents the metabolic pathway (simplified) when pcDNA is injected into the oocytes. During this project it was observed that mRNA yielded greater expression than pcDNA so it was the preferred vector. b, Shows the basic anatomy of the Xenopus oocyte. The follicular is removed before transfection, pcDNA is injected into the animal pole because that is where the nucleus is located. mRNA can be injected into either the animal or vegetal pole (Bianchi and Driscoll, 2006).

2.6.1 Oocyte preparation

Xenopus oocytes were prepared for DNA/mRNA injection by treating them with 10 ml of Barth's gentamicin theophylline pyruvate (GTP) (free of calcium) with a collagenase concentration of 250µg/ml. Ca^{2+} free Barth's GTP is used as Ca^{2+} is a catalyst for the tissue dissociation enzyme collagenase, the removal of Ca^{2+} helps control the reaction and makes the complete lysis of the oocytes less likely. The oocytes were then placed on a roller mixer for ~ 60 minutes or until the oocytes have separated and the connective tissue has been broken down at 19 -21°C. The oocytes were rinsed with Barth's GTP (free of Calcium) a minimum of 3 times or until the solution was transparent. The oocytes were then placed in a petri dish of Barth's GTP (containing Ca2+) for ~ 24 hours at 19 -21°C. Using a light microscope at an appropriate magnification the extrafollicular layer was removed using

forceps that have been sanitised with 70% ethanol. Once the extrafollicular has been removed they were placed into another petri dish with Barth's GTP containing Ca^{2+} and stored at 19 -21°C.

2.6.2 Oocyte Transfection

The nanolitre injection system (WPI, Nanoliter 2010 injector) was setup in preparation for injection. The needle was fully extended, glass capillaries (WPI, Glass capillaries, 504949) were pulled using the P-97 Flaming/Brown sutter instrument (figure 2.6.2.1) and the tip was cut to ~25µM in diameter forming a glass needle. The capillary was filled with paraffin oil to provide increase hydrostatic pressure and fitted onto the nanoliter injector (figure 2.6.2.2). 1.5 µl of DNA/mRNA of each of subunit with a concentration of 100 – 250 µg/µl in a complementary combination was pipetted on the surface of sterile petri dish, i.e 1.5 µl GRIN1A and 1.5 µl of GRIN2A. A pipette was used to mix the 3 µl of genetic material. The 3 µl was drawn into the glass needle in bursts after it had been manoeuvred into the solution, this lowers the chance of drawing in air. Once nearly all of the DNA/mRNA was drawn up, the custom petri dish (figure 2.6.2.3) was filled to a 1/3 with Ca^{2+} containing Barth's GTP and the previously separated oocytes were placed in the grooves. 50 nl of DNA/mRNA was injected into each oocyte, DNA was injected into the animal pole while mRNA was injected into either the animal or vegetal pole. once all the oocytes in the petri dish had been injected they were transferred to a 24 well costar. One oocyte in each well and the wells were filled withCa^{2+} Barth's GTP. Damaged oocytes were removed and those that remained were incubated at 19 – 21°C for 2 days before being stored at 2 – 8°C.

Figure 2.6.2.1: P-97 Flaming/Brown, Sutter Instruments Co. US

Figure 2.6.2.2: WPI, Nanoliter Injector 2010, Used for oocyte transfection

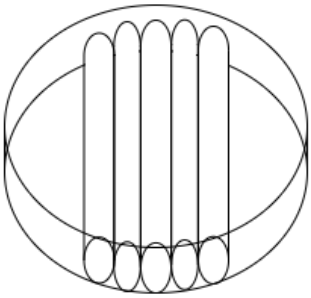

Figure 2.6.2.3: A custom petri dish. The tubing is fixed in place. Its design makes DNA/RNA injection easier as the oocytes are placed in the grooves of the tubing.

2.7 Electrophysiology

2.7.1 Two-electrode Voltage Clamp

Two-electrode voltage clamp (TEVC) is a technique used to record the electrical currents across the membrane. The membrane potential/voltage is “clamped” at a certain value by injecting a current of the same amplitude but reversed polarity.

Microelectrodes were pulled from glass capillaries (GC150TF-10, Harvard Apparatus, US) using the P-97 Flaming/Brown puller. The Teflon was removed from coated silver wire (AG549711, Advent Research materials Ltd, UK) and the exposed silver was coated in silver chloride (AgCl) via electrolysis. The microelectrodes were ~2/3 filled with 3 M KCl with a resistance of 0.5 – 2 MΩ. The AgCl coated silver wire and microelectrode were attached to the headstage (figure 2.7.1.1). *Xenopus* ringer solution was primed through a multi-channel gravity fed perfusion system and controlled through a valvlink™ 8 interface. The headstages were connected to the GeneClamp 500B amplifier which can adjust gain, stability and holding potential, it was also connected to an A/D converter (Digidata). The software used to record the changes in membrane current was WinEDR v5.5.4 (University of Strathclyde, UK).

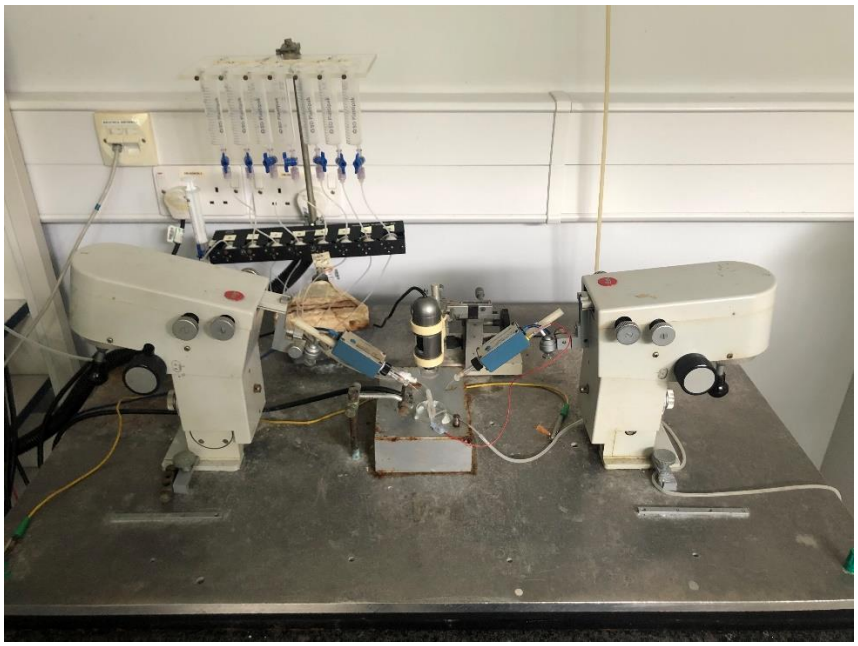

Figure 2.7.1.1: TEVC setup. A transfected oocyte is placed in the perfusion chamber where it then exposed to varying concentrations of drugs and physiological solution (Xenopus ringer) through a multi-channel perfusion system. The microelectrodes were connected to the headstages which were connected to geneclamp 500B amplifier and the digidata A/D converter. This setup was connected to a PC.

2.8 Experimental procedure

The injected oocytes were at membrane potentials -25 mV, -50 mV, -75 mV and -100 mV and while they are in the perfusion chamber where they were constantly exposed to Xenopus ringer running the perfusion system at a rate of ~ 5 ml/min. The agonist solution (10^{-4} M NMDA, 10^{-5} M Glycine diluted in *Xenopus* ringer) was made from 10^{-2} M NMDA in *Xenopus* ringer (stored at -20°C) and 10^{-2} M of Glycine in *Xenopus* ringer made fresh every day of testing. Memantine was made into a 10^{-2} M stock solution diluted in *Xenopus* ringer(stored at -20°C). From the stock solution a 10^{-4} M memantine test solution using the agonist (10^{-4} M NMDA, 10^{-5} M Glycine). Via a 1/10 serial dilution with the agonist 10^{-5} M, 10^{-6} M, 10^{-7} M, and 10^{-8} M test solutions were made.

From the HAE glass ampoules, a 3 mg/ml stock solution was made by adding 333 µl of DMSO which can be stored at -20°C. The stock solution was then diluted to 3 µg/ml with the agonist (10^{-4} M NMDA, 10^{-5} M Glycine) for the highest test solution, then via a 1/10 serial dilution with the agonist 0.300 µg/ml, 0.030 µg/ml, and 0.003 µg/ml all of which will be used to measure inhibition.

A harmonine analogue was also tested, this variable was to investigate which structural features of harmonine are responsible for its inhibitory properties. The analogue coded ACB-6-90 (Figure 2.8.1) has changed the location of one of the amine groups. The analogue was supplied by the University of Tasmania, Australia in powder form to be stored at -20°C. A stock solution was made to 0.0097 M by adding 3 ml DMSO and 928 µl HCl, the use of HCL was to allow the analogue to dissolve as it may have formed a free-base in the solution and became insoluble. From the stock solution a 10^{-4} M solution was made by diluting it in an agonist solution (10^{-4} M NMDA, 10^{-5} M Glycine). From this concentration via serial dilution 10^{-5} M, 10^{-6} M and 10^{-7} M were made for testing.

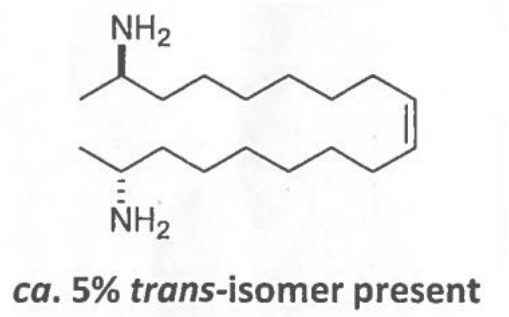

Figure 2.8.1 ACB-6-90 Harmonine Analogue. The position of one of the amine groups has changed from the first carbon to the second carbon in the chain.

2.9 Statistical analysis

The data was collected through WinEDR version 5.5.4 and tabulated in Microsoft Office Excel, the analysis and formation of graphs was conducted using Graphpad Prism (Graphpad software, LLC) version 9.4.1. When measuring the change in current it was the steady state/late current (figure 2.9.1) that was measured, as the inward and outward current has reached equilibrium. The data was normalised using the mean of the maximal response as the 100% point.

IC_{50} was calculated using the normalised data of each variable group and log concentrations. "log(inhibitor) vs. normalized response - Variable slope" which was a non-linear regression curve fit. IC_{50} equation 1:

$$\% \text{ Control response} = \frac{100}{1+10^{(\text{LogIC50-X})*\text{HillSlope}}}$$

X is the concentration of the inhibitor. This equation was used to calculate the IC_{50} of Memantine and ACB-6-90.

IC_{50} equation 2:

$$\% \text{ Control response} = \frac{100}{1+(IC_{50}/X)^{\text{HillSlope}}}$$

This equation was used to calculate the IC_{50} of HAE.

Voltage dependence was calculated by using non-linear regression with an adaptation of Woodhull's equation for ion permeability (1973) to fit IC_{50} against holding potential.

$$Y = \frac{IC_{50}\text{zero}(\exp(\text{zDELTA}(X/1000)*F))}{RT}$$

zDELTA is the slope and z is the charge of the molecule. For memantine z = 1, for HAE and ACB-6-90 z = 2. The initial values for zDELTA was 0.5 for memantine and 1 for HAE and ACB-6-90 and IC_{50}zero was 5. F is Faradays constant and equals 96485 C/mol, R is the universal gas constant = 8.314 J K^{-1} mol^{-1}, and T absolute temperature = 297 K.

IC_{50} values were compared for significance using an extra-sum of squares F-test on Graphpad prism.

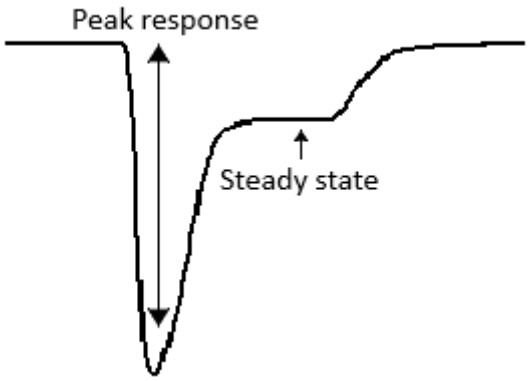

Figure 2.9.1: Features of a typical GluN1A-GluN2A response

3 Results

3.1 Electrophysiological Recordings at Various different holding potentials

Xenopus oocytes were injected with mRNA for the subunit combinations GluN1A-GluN2A and GluN1A-GluN2B. The oocytes that were injected with GluN1A-GluN2B mRNA did not show significant expression so any data or results from that receptor were excluded from this report. The GluN1A-GluN2A injected oocytes exhibited significant expression of functional NMDARs for electrophysiological recordings. To ensure that the activity recorded was due to NMDARs present in the membrane, un-transfected oocytes were tested with the agonist solution. An inward current was not observed from this test. To confirm NMDAR expression the agonist solution (10^{-4} M NMDA and 10^{-5} M glycine) was applied to the injected oocytes while the perfusion system and response was measured using TEVC. To investigate the current-voltage relationship of GluN1A-GluN2A receptors the agonist was applied at several membrane/holding potentials (figure 3.1.1).

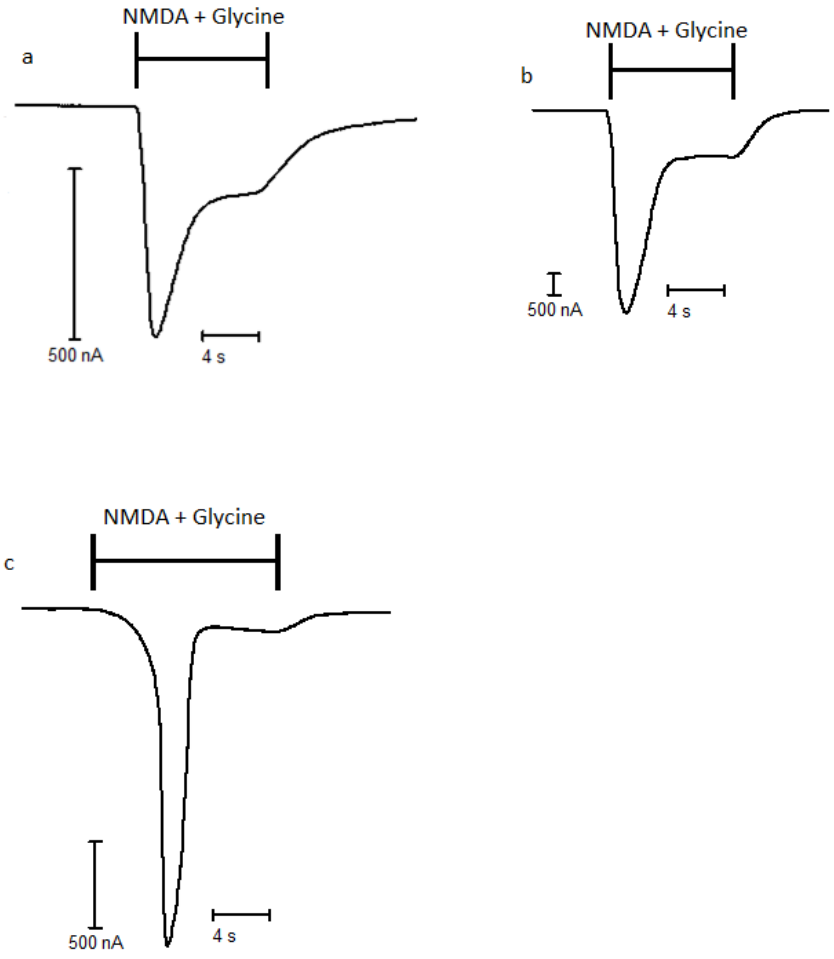

Figure 3.1.1: Agonist (10^{-4} M NMDA and 10^{-5} M glycine) responses of GluN1A-GluN2A receptors expressed in *Xenopus* oocytes. The traces are from WinEDR and represent the change in current in response to application of the agonist at varying membrane potentials. (a) is the response at a holding potential of -50 mV, (b) -75 mV and (c) -100 mV.

The application of the agonist (10^{-4} M NMDA and 10^{-5} M glycine) resulted in a negative inward current and its amplitude varied depending on the membrane potential (figure 3.1.2). The smallest current was observed at -100 mV with a mean of 44.66 nA (n = 6) and -75 mV was the largest with a mean of 354.61 nA (n = 6), excluding -100 mV there was an increase in amplitude as the membrane potential became more negative. A larger current was observed at -75 mV compared to -50 mV with a mean of 180.08 nA (n = 5), but the response at -50 mV was larger than the response at -100 mV. The shape of the curve varied along with the membrane potential. Observed at more negative potentials was a larger peak response relative to the steady state (figure 3.1.1)

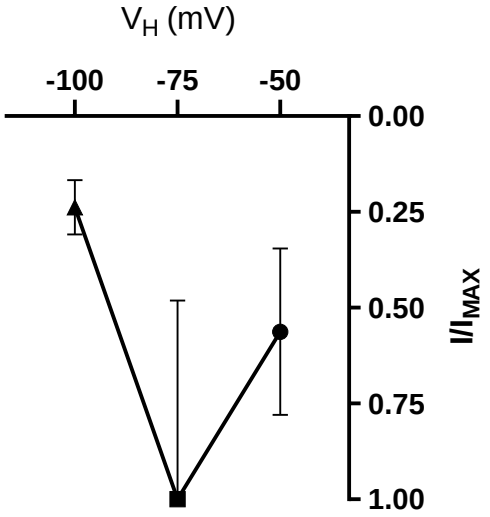

Figure 3.1.2: The mean current-voltage relationship of GluN1A-GluN2A expressed in *Xenopus* oocytes. I/I_{MAX} calculated at -50, -75 and -100 mV (n= 5-8) These data points are not statistical different (Kruskal-Wallis test P = 0.5941). Data points at a holding voltage of -25 mV were excluded due to a small sample size (n=2).

3.2 The concentration-dependent effect of memantine on GluN1A-GluN2A receptors expressed in *Xenopus* oocytes.

It was observed that the application of memantine at different concentrations inhibits GluN1A-GluN2A receptors in a concentration-dependent manner. As the concentration of memantine is increased, it further reduces the response of the NMDAR, with 10^{-8} M barely inhibiting the receptor's response and 10^{-4} M nearly achieving complete inhibition (figure 3.2.1). This concentration-dependent inhibition was also present at different membrane potentials (figure 3.2.3). At every holding potential tested (-50, -75, and -100 mV) memantine concentration has different effects on response inhibition, with the largest reduction in response triggered by the application of 10^{-6} M and 10^{-5} M memantine. The IC_{50} equation 1 was used to quantify memantine's inhibition at different holding potentials by fitting a curve on a log[concentration] vs % control response graph (figure 3.2.2).

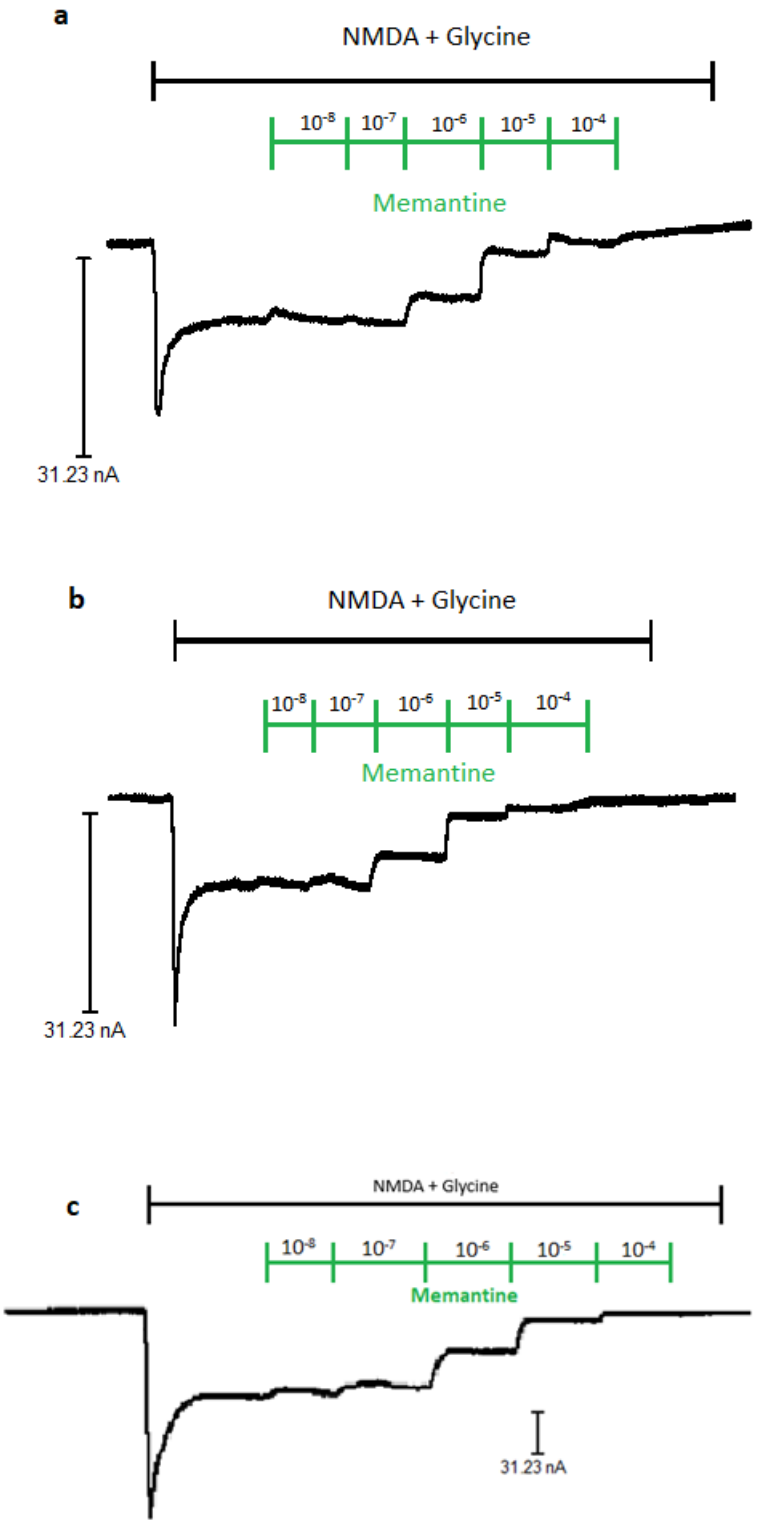

Figure 3.2.1: Electrophysiological response of different concentrations of memantine on GluN1A-GluN2A. An agonist response was recorded first by applying the 10^{-4} NMDA + 10^{-5} glycine solution (black bar), once the response plateaued memantine concentrations 10^{-8} M – 10^{-4} M (green bars)

were applied till the response plateaued. A) is a response from an oocyte at a -50 mV holding potential. B) The response at -75 mV. C) the response was taken at -100 mV.

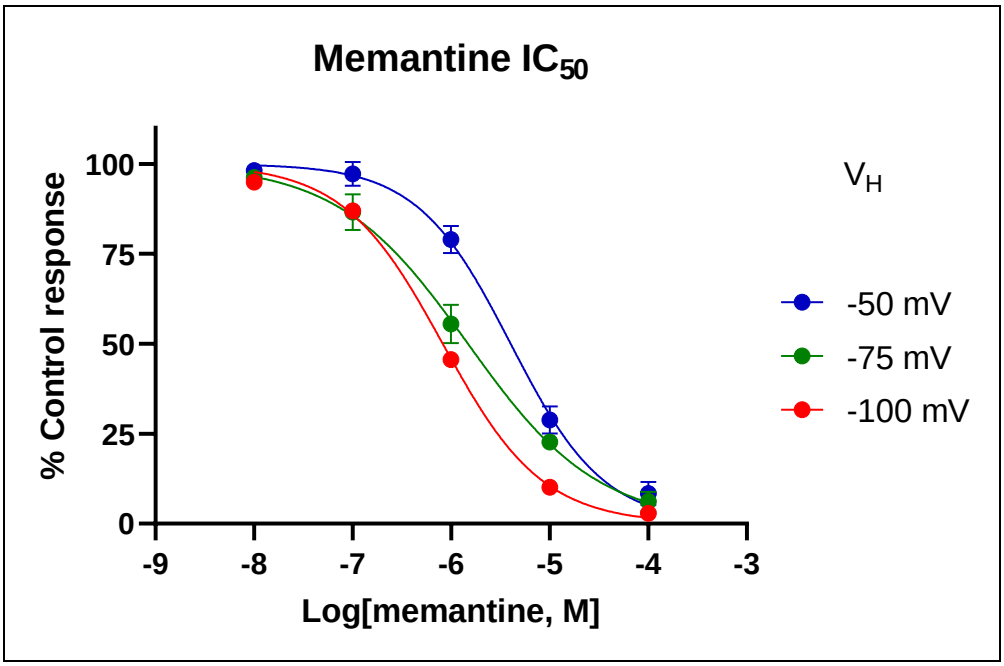

Figure 3.2.2: Memantine concentration-inhibition curves of GluN1A-GluN2A receptors at varying holding potentials. The responses to memantine concentrations 10^{-8} M – 10^{-4} M when applied until the current plateaus. The agonist (10^{-4} M + 10^{-5} glycine) was applied first as it functions as a control response to the reduced responses to the varying memantine concentrations. The data points represent the mean ± SEM of the memantine steady-state currents depicted as a percentage (%) of the control response. Curves were fitted with the IC_{50} equation. The inhibition at different holding potentials were assessed -50 mV, n=5 (blue), -75 mV, n=5 (green) and -100 mV, n=6 (red).

Table 3.2.1: Memantine IC_{50} values for GluN1A-GluN2A at varying membrane potentials. The IC_{50} values were calculated from the fitted curves in figure 3.2.2. All differences were $p < 0.0001$, assessed with an extra sum of squares F-test.

Memantine	IC_{50} (µM)		
NMDAR	-50 mV	-75 mV	-100 mV
GluN1A-GluN2A	4.02 (3.072 – 5.256)	1.482 (1.053 – 2.088)	0.8277 (0.7696 – 0.8794)

A positive correlation between membrane potential and IC_{50} was observed, so as the membrane became more negative memantine's IC_{50} decreased. For GluN1A-GluN2A receptors the lowest memantine potency was at the membrane potential -50 mV 4.02 µM (3.072 µM – 5.256 µM), the most potent being at -100 mV with an IC_{50} of 0.8277 µM (0.7696 µM – 0.8794 µM). An extra sum of squares F-test comparing the IC_{50} values two data sets at a time found all values to be significantly different from one another, $p < 0.0001$. The data suggests that at less negative membrane potentials memantines inhibition is less potent and is voltage-dependent for the GluN1A-GluN2A receptor.

Figure 3.2.3 is an analysis of the relationship between memantine IC_{50} and holding potential. A curve was fitted to the data shown in figure 3.2.3 by using the voltage-dependence equation. The data shown in figure 3.2.3 suggests that memantine inhibition is more potent at more negative membrane potentials but the voltage-dependence curve has a slope (zDELTA) of 0.9249 with a p-value of 0.058. This demonstrates that membrane potential has no significant effect on memantine potency on GluN1A-GluN2A receptors.

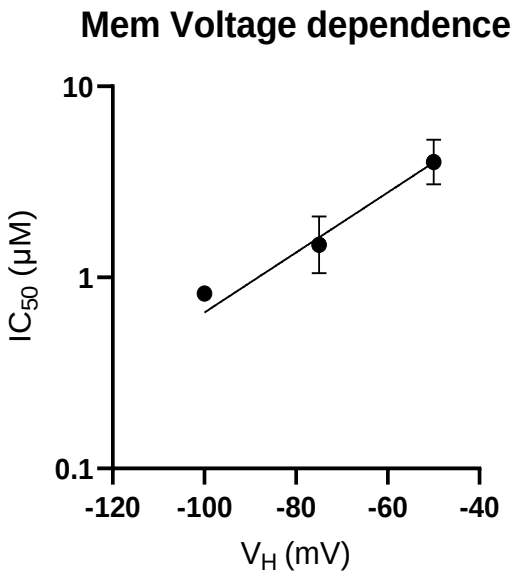

Figure 3.2.3: Memantine voltage dependence, IC_{50} (µM) plotted against holding potential (mV). (a) is plot of the IC_{50} data points for the holding potentials -50 mV (n=5), -75 mV (n=5) and -100 mV (n=6). A curve was fitted onto (a) using the voltage-dependence equation where the initial value for zDELTA = 0.5 represents the charge on memantine, p = 0.058.

The effect of memantine on signal decay (τ) functions in a concentration-dependent manner was measured. At lower memantine concentrations (10^{-8} M and 10^{-7} M) the signal decay was larger. At a holding potential of -100 mV, τ is 845.6 ms (10^{-8} M) and 765.55 ms (10^{-7} M), at -50 mV τ is 712.75 ms (10^{-8} M) and 1198.50 ms (10^{-7} M) (table 3.2.2). At both holding

potentials τ exhibits a concentration dependent decrease and the largest decrease in τ occurs at 10^{-6} M to 10^{-5} M, -100 mV, 702.78 ms (10^{-6} M) to 480.47 ms (10^{-5} M), -50 mV, 723.73 ms (10^{-6} M) to 364.10 ms (10^{-5} M). Table 3.2.2 demonstrates that there is a general decrease in τ as concentration increases with the exception of memantine 10^{-7} M at -50 mV which increases to 1198.50 ms from 712.75 ms (10^{-8} M).

Table 3.2.2: Memantine signal decay. The mean signal decay of memantine concentrations 10^{-8} M – 10^{-4} M at holding potentials of -50 (n = 4) and -100 mV (n = 5). measured in milliseconds using WinWCP V5.7.1 (University of Strathclyde, UK)

V_H (mV)	Log[Memantine, M]	τ (ms)
-100	10^{-8}	845.60 ± 17.86
	10^{-7}	765.55 ± 18.70
	10^{-6}	702.78 ± 2.90
	10^{-5}	480.47 ± 3.91
	10^{-4}	320.92 ± 4.48
-50	10^{-8}	712.75 ± 68.17
	10^{-7}	1198.50 ± 0.85
	10^{-6}	723.73 ± 2.58
	10^{-5}	364.10 ± 3.07
	10^{-4}	210.55 ± 5.19

3.3 The concentration-dependent effect of *H. axyridis* alkaloid extract (HAE) on GluN1A-GluN2A receptors expressed in *Xenopus* oocytes.

It was observed that the application of HAE at different concentrations inhibits GluN1A-GluN2A receptors in a concentration-dependent manner. As the concentration of HAE increases the response (steady state) of the NMDAR decreases. 0.003 μg/ml barely inhibits the receptor response and 3 μg/ml nearly achieves complete inhibition (figure 3.3.1). This concentration-dependent inhibition was also present at different membrane potentials (figure 3.3.2). At every holding potential tested (-25, -50, -75, and -100 mV) HAE concentration influences response inhibition, with the largest reduction in response triggered by the application of 0.3 μg/ml and 3 μg/ml HAE. The IC_{50} equation 2 was used to quantify HAE's inhibition at different holding potentials by fitting a curve on a concentration vs % control response graph (figure 3.3.3).

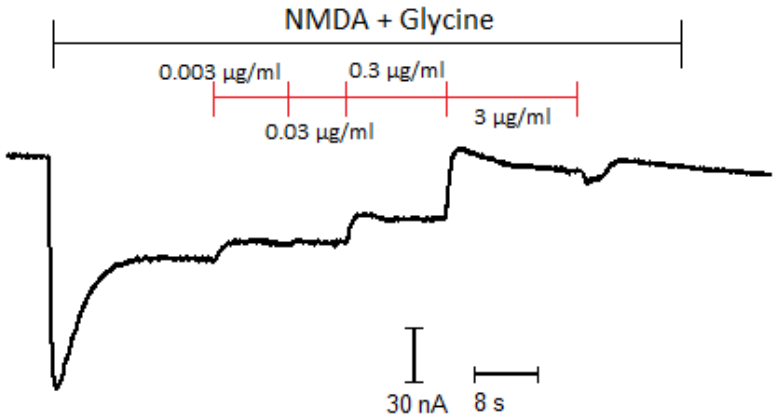

Figure 3.3.1: Electrophysiological response of different concentrations of HAE on GluN1A-GluN2A. An agonist response was recorded first by applying the 10^{-4} NMDA + 10^{-5} glycine solution (black bar), once the response plateaued memantine concentrations 0.003 µg/ml – 3.000 µg/ml (red bars) were applied till the response plateaued. This response was taken from an oocyte at a holding potential of -75 mV.

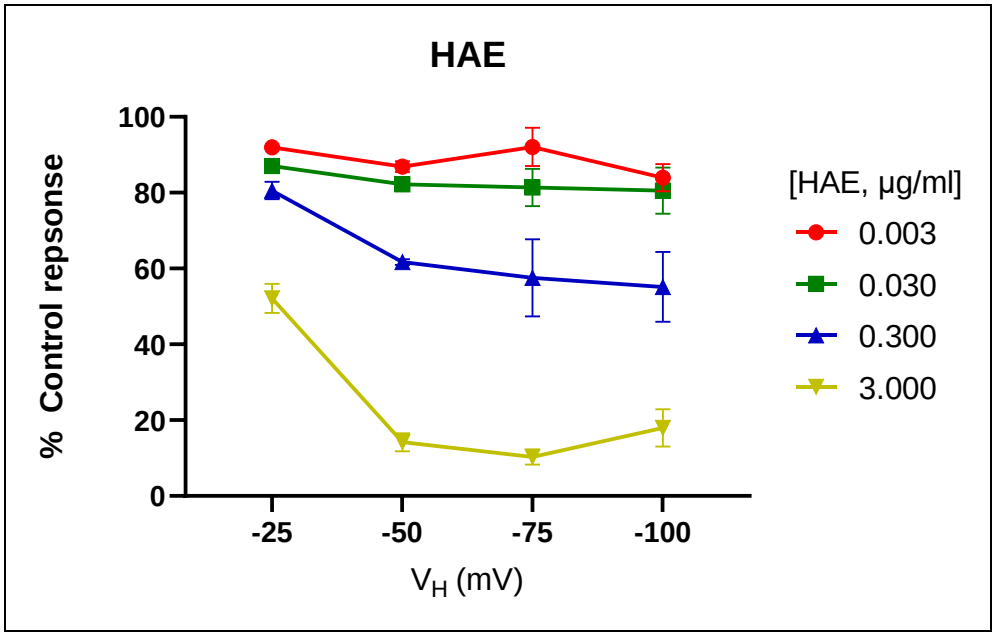

Figure 3.3.2: Demonstration of the holding potential vs control response relationship. The mean ± SEM % control response of HAE concentrations 0.003 µg/ml – 3 µg/ml were plotted at the holding potentials -25mV, -50 mV, -75 mV and -100 mV for GluN1A-GluN2A receptors expressed in *Xenopus* oocytes. The data points depict the late current of the HAE response and (%) percentage of mean agonist (10^{-4} NMDA + 10^{-5} glycine) response which is the control. The sample size for all conditions was n ≥ 3.

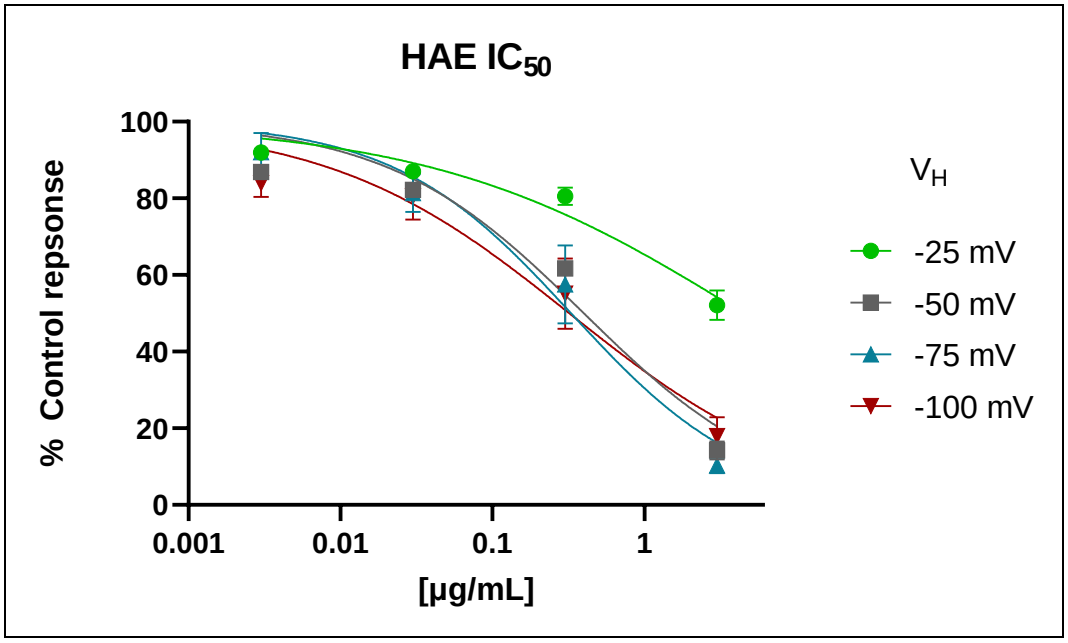

Figure 3.3.3: HAE concentration-inhibition curves of GluN1A-GluN2A receptors at varying holding potentials. The responses to HAE concentrations 0.003 µg/ml – 3.000 µg/ml when applied until the current plateaus. The agonist (10^{-4} M + 10^{-5} glycine) was applied first as it functions as a control response to the reduced responses caused by varying HAE concentrations. The data points represent the mean ± SEM of the HAE steady-state currents depicted as a percentage (%) of the control response. Curves were fitted with the IC_{50} equation. The inhibition at different holding potentials were assessed -25 mV, n=3 (green) -50 mV, n=5 (grey), -75 mV, n=5 (blue) and -100 mV, n=6 (dark red).

Table 3.3.1: HAE IC_{50} values for GluN1A-GluN2A at varying membrane potentials. The IC_{50} values were calculated from the fitted curves in figure 3.3.3. All IC_{50} values when compared to -25 mV were $p < 0.0001$, -50, -75 and -100 mV when compared to each other $p > 0.05$. Assessed with an extra sum of squares F-test.

HAE	IC_{50} (µg/ml)			
	-25 mV	-50 mV	-75 mV	-100 mV
GluN1A-GluN2A	4.473 (2.531 – 10.97)	0.3988 (0.2810 – 0.5601)	0.3286 (0.1786 – 0.5867)	0.3199 (0.1480 – 0.6977)

There was a positive correlation between membrane potential and IC_{50}, so as membrane potential became more negative, HAE IC_{50} decreased. For GluN1A-GluN2A receptors the lowest HAE potency was at a membrane potential of -25 mV 4.473 µg/ml (2.531 µg/ml – 10.97 µg/ml), the most potent being at -100 mV with an IC_{50} of 0.3199 µg/ml (0.1480 µg/ml – 0.6977 µg/ml). An extra sum of squares F-test comparing the IC_{50} values two data sets at a

time found the IC_{50} values for -50 mV (0.3988 µg/ml), -75 mV (0.3286 µg/ml), -100 mV (0.3199 µg/ml) were significantly different from -25 mV (4.473 µg/ml), $p < 0.0001$. The IC_{50} values for -50 mV, -75 mV and -100 mV are not significantly different, $p > 0.05$. The data suggests that at less negative membrane potentials HAE's inhibition is less potent that HAE is voltage-dependent for the GluN1A-GluN2A receptor.

Figure 3.3.4 is an analysis of the relationship between HAE IC_{50} and holding potential. A curve was fitted to the data shown in figure 3.3.4 (a) by using the voltage-dependence equation. The data shown in figure 3.3.4 suggests that HAE inhibition is more potent at more negative membrane potentials. The voltage-dependence curve has a slope (zDELTA) of 2.311 with a p-value of 0.0072. This demonstrates that membrane potential has a significant effect on HAE potency on GluN1A-GluN2A receptors.

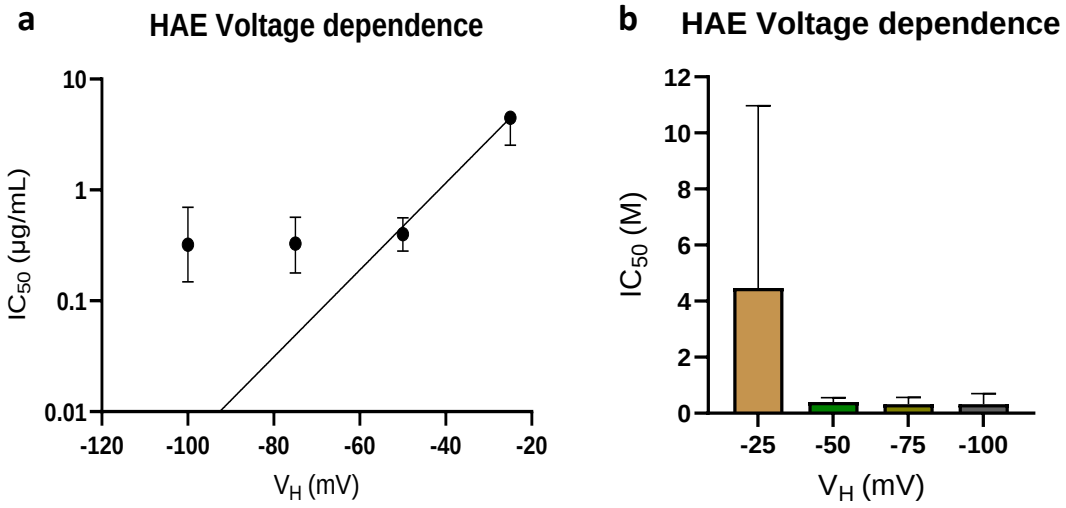

Figure 3.3.4: HAE voltage dependence, IC_{50} (µM) plotted against holding potential (mV). (a) is plot of the IC_{50} data points for the holding potentials -25 mV (n=3), -50 mV (n=5), -75 mV (n=5) and -100 mV (n=3). A curve was fitted onto (a) using the voltage-dependence equation where the initial value for zDELTA (slope) = 1 as it incorporates the charge on HAE. (b) is the bar chart representation of the relationship between IC_{50} and holding potential. $p = 0.0072$.

The effect of HAE on signal decay (τ) functions in a concentration-dependent manner. At lower HAE concentrations (0.003 µg/ml and 0.03 µg/ml) the signal decay is larger. At a holding potential of -50 mV, τ is 1072.12 ms (0.003 µg/ml) and 764.30 ms (0.03 µg/ml), at -75 mV, τ is 1036.33 ms (0.003 µg/ml) (table 3.3.2). At both holding potentials, τ exhibits a concentration-dependent decrease (figure 3.3.5) and the largest decrease in τ occurs from 0.003 µg/ml (1072.12 ms) to 0.03 µg/ml (764.30 ms) at -50 mV. At -75 mV the sample size of viable data for HAE concentration 0.03 µg/ml was too small (n < 3). Figure 3.3.5 demonstrates that there is a general decrease in τ as concentration increases.

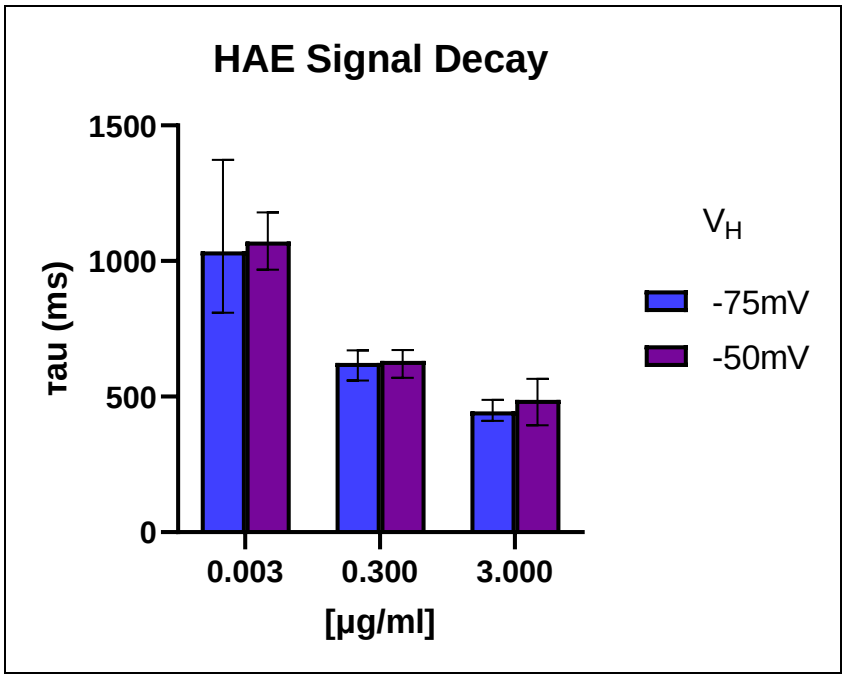

Figure 3.3.5: HAE signal decay. The mean ± SEM signal decay of HAE concentrations 0.003 µg/ml, 0.3 µg/ml and 3 µg/ml at holding potentials of -50 and -75 mV. Measured in milliseconds using WinWCP V5.7.1 (University of Strathclyde, UK).

Table 3.3.2: HAE signal decay. The mean signal decay of HAE at 0.003 µg/ml – 3 µg/ml at holding potentials -50 mV (n = 4) and – 75 mV (n = 3) (excluding 0.03 µg/ml at -75 mV due a small sample size, n =1). Signal decay was measured in milliseconds using WinWCP V5.7.1 (University of Strathclyde, UK).

V_H (mV)	[HAE, µg/ml]	τ (ms)
-75	0.003	1036.33 ± 7.92
	0.030	- ± -
	0.300	624.70 ± 3.50
	3.000	446.10 ± 2.51
-50	0.003	1072.12 ± 10.84
	0.030	764.30 ± 20.32
	0.300	631.50 ± 4.84
	3.000	487.64 ± 2.87

3.4 The concentration-dependent effect of the harmonine (analogue ACB-6-90) on GluN1A-GluN2A receptors expressed in *Xenopus* oocytes

ACB-6-90 at different concentrations inhibits GluN1A-GluN2A receptors in a concentration-dependent manner. As the concentration of ACB-6-90 is increased it further reduces the response of the NMDAR, with 10^{-7} M barely inhibiting the receptors response and 10^{-4} M nearly achieving complete inhibition (figure 3.4.1). This concentration-dependent inhibition was also present at different membrane potentials (figure 3.2.2). At both holding potentials tested (-50 and -75 mV) ACB-6-90 concentration has a direct effect on response inhibition, with the largest reduction in response triggered by the application of 10^{-6} M and 10^{-5} M ACB-6-90 (figure 3.4.1). The IC_{50} equation 1 was used to quantify ACB-6-90's inhibition at both holding potentials by fitting a curve on a log[concentration] vs % control response graph (figure 3.4.3).

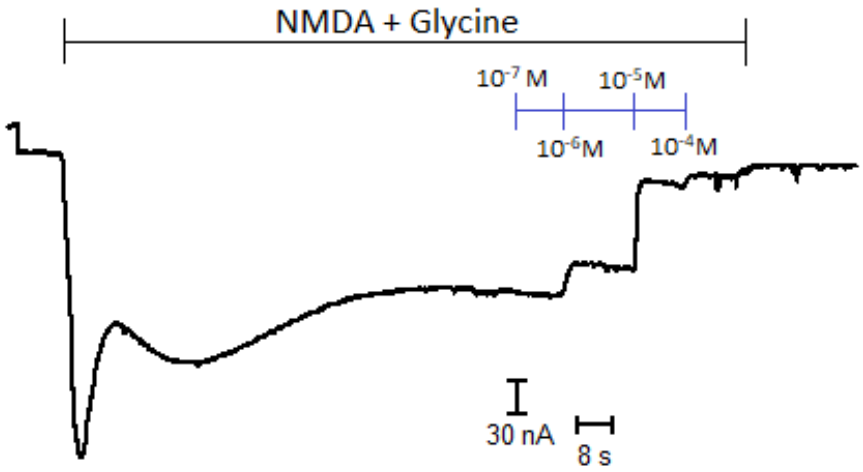

Figure 3.4.1: Electrophysiological response of different concentrations of ACB-6-90 on GluN1A-GluN2A. An agonist response was recorded first by applying the 10^{-4} NMDA + 10^{-5} glycine solution (black bar), once the response plateaued ACB-6-90 concentrations 10^{-7} M – 10^{-4} M (blue bars) were applied till the response plateaued. This response was taken from an oocyte at a holding potential of -75 mV.

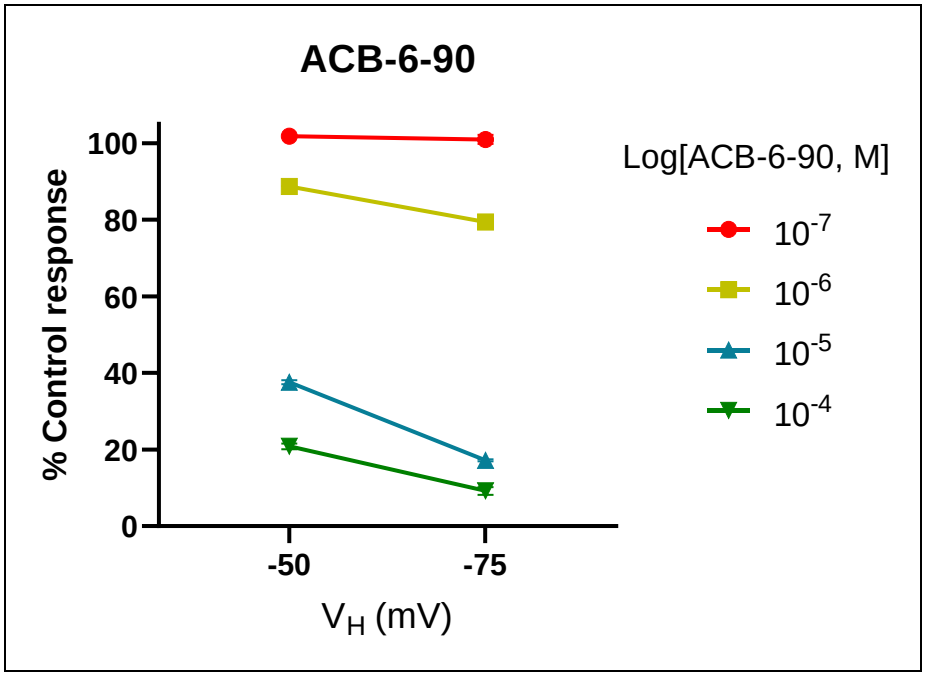

Figure 3.4.2: Demonstration of the holding potential vs control response relationship. The mean ± SEM % control response of ACB-6-90 concentrations 10^{-7} M – 10^{-4} M was plotted at the holding potentials -50 mV and -75 mV for GluN1A-GluN2A receptors expressed in *Xenopus* oocytes. The data points depict the late current of the ACB-6-90 response and (%) percentage of mean agonist (10^{-4} NMDA + 10^{-5} glycine) response which is the control. The sample size for all conditions was n = 3.

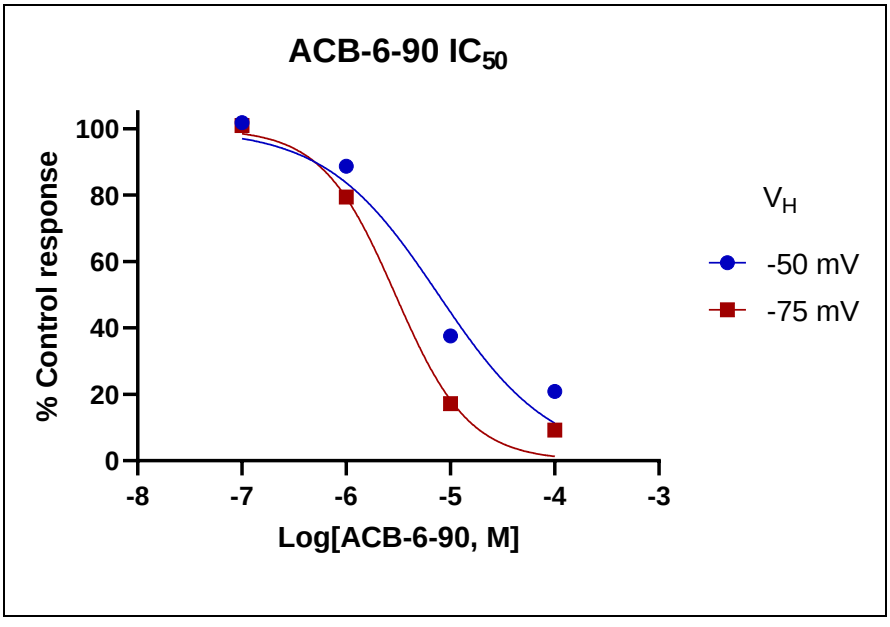

Figure 3.4.3: ACB-6-90 concentration-inhibition curves of GluN1A-GluN2A receptors at varying holding potentials. The responses to ACB-6-90 concentrations 10^{-7} M – 10^{-4} M when applied until the current plateaus. The agonist (10^{-4} M + 10^{-5} glycine) was applied first as it functions as a control response to the reduced responses to the varying ACB-6-90 concentrations. The data points represent the mean ± SEM of the ACB-6-90 steady-state currents depicted as a percentage (%) of the

control response. Curves were fitted with the IC_{50} equation. The inhibition at different holding potentials were assessed -50 mV, n=3 (blue), -75 mV, n=3 (red).

Table 3.4.1: ACB-6-90 IC_{50} values for GluN1A-GluN2A at varying membrane potentials. The IC_{50} values were calculated from the fitted curves in figure 3.4.3. The difference was significant, p = 0.0003, assessed with an extra sum of squares F-test.

ACB-6-90	IC_{50} (μM)	
	-50 mV	-75 mV
GluN1A-GluN2A	7.695 (5.120 – 11.91)	2.969 (2.357 – 3.739)

The data revealed a positive correlation between membrane potential and IC_{50}. As the membrane became more negative ACB-6-90's IC_{50} decreased. For GluN1A-GluN2A receptors the lowest ACB-6-90 potency was at the membrane potential -50 mV 7.695 μM (5.120 μM – 11.91 μM), the most potent being at -75 mV with an IC_{50} of 2.969 μM (2.357 μM – 3.739 μM). An extra sum of squares F-test compared the two data sets and found them to be significantly different from one another, p = 0.0003. The data suggests that at less negative membrane potentials ACB-6-90s inhibition is less potent and is voltage-dependent for the GluN1A-GluN2A receptor.

Figure 3.4.4 is an analysis of the relationship between memantine IC_{50} and holding potential. A curve was fitted to the data shown in figure 3.4.4 (a) by using the voltage-dependence equation. The data shown in figure 3.4.4 suggests that ACB-6-90 inhibition is more potent at more negative membrane potentials, but the voltage-dependence curve was unable to calculate a p-value, the slope (zDELTA) was 0.9749. This would suggest that in amongst these data sets membrane potential has no significant effect on ACB-6-90 potency on GluN1A-GluN2A receptors.

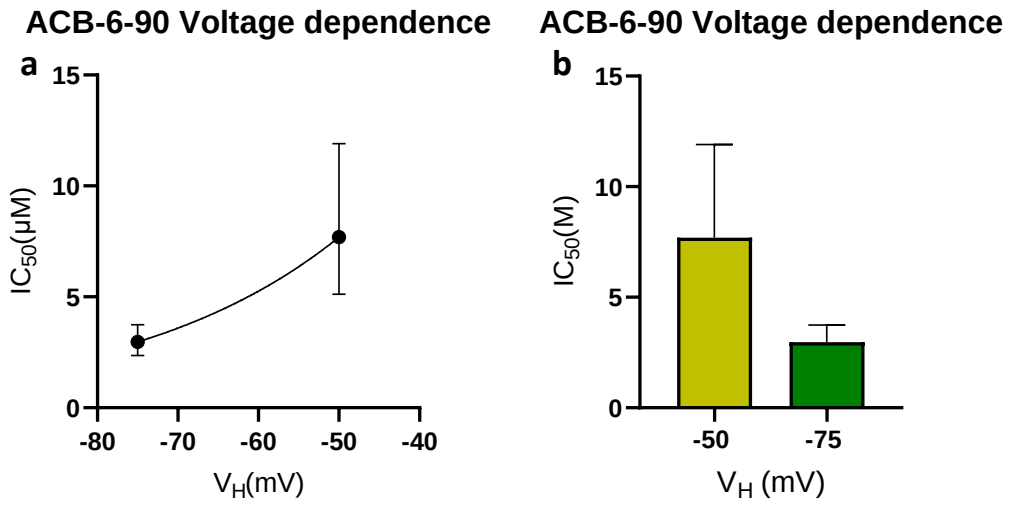

Figure 3.4.4: ACB-6-90 voltage dependence, IC_{50} (μM) plotted against holding potential (mV). (a) is plot of the IC_{50} data points for the holding potentials -50 mV (n=3) and -75 mV (n=3). A curve was fitted onto (a) using the voltage-dependence equation where the initial value for zDELTA (slope) = 1 as it incorporates the charge on ACB-6-90. (b) is the bar chart representation of the relationship between IC_{50} and holding potential. p = unable to calculate, $R^2 = 1$.

The effect of ACB-6-90 on signal decay (τ) functions in a concentration-dependent manner. At lower ACB-6-90 concentrations (10^{-6} M) the signal decay is larger. At a holding potential of -100 mV, τ is 1049.47 ms (10^{-6} M), at -50 mV τ is 829.10 ms (10^{-6} M) (table 3.4.2). At both holding potentials, τ exhibits a concentration-dependent decrease (figure 3.4.5) and the largest decrease in τ occurs at 10^{-6} M to 10^{-5} M, -100 mV, 1049.47 ms (10^{-6} M) to 685.33 ms (10^{-5} M), -50 mV, 829.10 ms (10^{-6} M) to 675.63 ms (10^{-5} M). Table 3.2.2 demonstrates that there is a general decrease in τ as concentration increases.

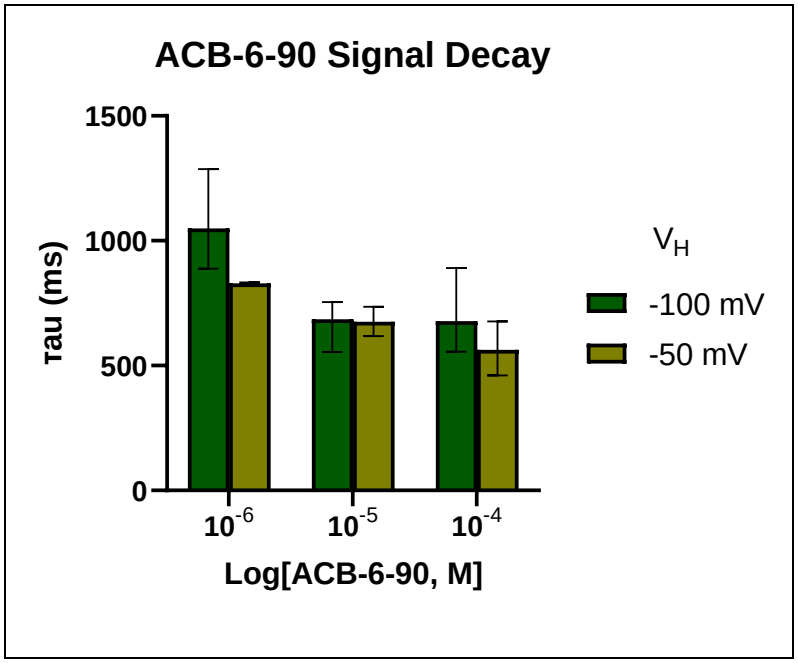

Figure 3.4.5: ACB-6-90 signal decay. The mean ± SEM signal decay of ACB-6-90 concentrations 10^{-6} M – 10^{-4} M at holding potentials of -50 (n = 3) and -100 mV (n = 3). Measured in milliseconds using WinWCP V5.7.1 (University of Strathclyde, UK).

Table 3.4.2: ACB-6-90 signal decay. The mean signal decay of ACB-6-90 concentrations 10^{-6} M – 10^{-4} M at holding potentials of -50 and -100 mV. 10^{-7} M was not included as the sample size was n = 2. measured in milliseconds using WinWCP V5.7.1 (University of Strathclyde, UK).

V_H (mV)	Log[ACB-6-90, M]	τ (ms)		
-100	10^{-7}	-	±	-
	10^{-6}	1049.47	±	5.14
	10^{-5}	685.33	±	1.49
	10^{-4}	677.97	±	3.30
-50	10^{-7}	-	±	-
	10^{-6}	829.10	±	4.80
	10^{-5}	675.63	±	1.22
	10^{-4}	563.43	±	1.50

4 Discussion

4.1 Memantine inhibition on GluN1A-GluN2A receptors expressed in *Xenopus laevis* oocytes

Memantine is an FDA-approved drug treatment for moderate to severe AD patients, and for the purposes of this study acts as a comparison for HAE. Memantine was shown to inhibit GluN1A-GluN2A receptors in a concentration-dependent manner but not in a voltage-dependent manner (figure 3.2.2, table 3.2.1 and figure 3.2.3). The highest concentration (10^{-4} M) nearly completely inhibited the agonist response (figure 3.2.1 and figure 3.2.2), so as expected the lower concentrations (10^{-8} M and 10^{-7} M) show minimal inhibition. In this study, the memantine IC_{50} value was calculated to be 1.48 µM at -75 mV (n=5). These results are similar to other studies that reported IC_{50} values of 1.25, 1.80 and 1.82 µM at holding potentials of -65 mV and -66 mV (Kotermanski, Wood and Johnson, 2009; Glasgow et al., 2017; Marotta et al., 2020). The differences between these values are small but they may have been the result of the different methods used such as patch clamp compared to TEVC used in this study, the model used, HEK293 cell lines instead of *Xenopus* laevis oocytes, and the use of rat NMDAR clones compared to human NMDAR clones. Despite these differences, the results are similar, and they also found memantine to have concentration-dependent behaviour. However Gilling et al., 2009 did use human GluN1A-GluN2A clones on HEK293 cell lines and found the memantine to be approximately 2 times as potency (0.79 µM) at a holding potential of -70 mV.

Voltage-dependence inhibition of GluN1A-GluN2A by memantine is one well-documented property of memantine (Blanpied et al., 1997; Gilling et al., 2009). In this study, the IC_{50} does vary depending on the membrane potential i.e., a membrane potential at -50 mV has an IC_{50} of 4.02 µM and a membrane at -100 mV has an IC_{50} of 0.83 µM. The data (without fitting a voltage-dependence curve) implies that memantine inhibits GluN1A-GluN2A in a voltage-dependent manner (table 3.2.1). Once the curve has been fitted the delta value = 0.92 and produces a voltage-dependence curve with a p-value of 0.058 (figure 3.2.3).

The line (figure 3.2.3) demonstrates that memantine inhibition decreases as the membrane becomes more positive, but these results may not be solely due to membrane voltage. The results state that the differences are not statistically significant so an open channel blocker mechanism may not describe memantine's mode of action. It may possible that there is some allosteric inhibition caused by memantine, meaning it must bind to a NMDAR site other than or including the pore. This kind of inhibition would decrease P_{OPEN} by altering channel kinetics, and is more dose dependent than voltage dependent as it less dependent on the pull of electrostatic attraction into the pore. Memantine is classed as an open channel blocker and voltage dependence is a feature of that class, memantine binds to the

pore of an open NMDAR to prevent Ca^{2+} influx, as the membrane potential becomes more negative electrostatic forces drive the open channel blocker to the membrane resulting in more 'trapped' memantine in the pore. These electrostatic forces increase the potency of the blocker. This study implies that this not the case and there may be some allosteric inhibition or that membrane voltage plays no role in memantine inhibition.

The onset (τ) of memantine was found to act in a concentration-dependent and voltage-dependent manner. At lower concentrations the decay is slower, a memantine concentration of 10^{-8} M at a membrane potential of -50 mV has a τ of 712.75 ms whereas at the same membrane potential but a concentration of 10^{-4} M τ is 210.55 ms (table 3.2.2). The effect of voltage is not as apparent as concentration yet is still present. At a memantine concentration of 10^{-4} M, at a membrane potential of -100 mV τ was 320.92 ms which is slower than 210.55 ms at -50 mV. Making the membrane more positive seems to decrease τ. The maximum therapeutic plasma concentration of memantine is 1 μM (10^{-6} M) in this study that concentration has a τ of 702.78 ms to 723.73 ms (Rammes, Danysz and Parsons, 2008).

4.2 *H. axyridis* alkaloid inhibition on GluN1A-GluN2A receptors expressed in *Xenopus laevis* oocytes

The main inhibitory component present in HAE is harmonine and is expected to be present at ~90%. Research by Patel, 2018 found that HAE antagonist effects on GluN1A-GluN2A, it was found that HAE functioned in similar concentration-dependent when compared to memantine which brought up the question does HAE block NMDARs in a similar manner to memantine. In this study, HAE inhibited GluN1A-GluN2A in a concentration-dependent manner 0.003 μg/ml barely inhibits the agonist response while a concentration of 3 μg/ml demonstrates inhibition of the response (figure 3.3.1 and figure 3.3.2). The concentration-dependent inhibition allowed for the calculation of IC_{50} values and fit of a concentration-inhibition curve (figure 3.3.3 and table 3.3.1). HAE was observed to be more potent at more negative membrane potentials. The least membrane potent potential was -25 mV with an IC_{50} of 4.473 μg/ml compared to the more potent 0.3199 μg/ml at a membrane potential of -100 mV. This compares to what was observed in memantine, so both molecules have the same concentration-dependent inhibition.

HAE demonstrated voltage-dependent inhibition (figure 3.3.4) as the membrane became more negative HAE became more potent as an inhibitor. This would suggest that HAE is an open channel blocker. The voltage-dependence analysis (figure 3.3.4) has a p-value of 0.0072 so the results are statistically significant and applicable, but the IC_{50} values from – 50 mV to -100 mV are not statistically different from one another. Using the extra sum of squares F-test it was calculated that the IC_{50} values for – 50 mV (0.3988 μg/ml), -75 mV

(0.3286 µg/ml) and -100 mV (0.3199 µg/ml) are not statistically different with p values of p > 0.05. This could mean that the mode of action of HAE on GluN1-2A receptors is that of an open channel blocker only from -25 mV to -50 mV. HAE could act as open channel blocker up to membrane potentials as negative as -50 mV, and potentials more negative it could act at allosteric sites or ligand sites to lower P_{OPEN} which inhibits ion influx. It may even be possible that there is a saturation effect in relation to electrostatic attraction of HAE to membrane which results in minimal differences in IC_{50} between more negative membrane potentials. More data is required to draw a more reliable conclusion

When comparing the potency of HAE in this study to other studies they are quite far apart, at -75 mV previous IC_{50} values for GluN1A-GluN2A were 0.179 µg/ml and 1.11 µg/ml (Patel, 2018; Kaur, 2022). 0.179 µg/ml is the most potent, then 0.3199 µg/ml and 1.11 µg/ml. Looking at values it would almost seem like 1.11 µg/ml is an outlier among them, but this is novel research so there is not a reliable number of studies to make a comparison, hence it is not possible at this moment in time to decide which value is the most accurate. It is also difficult to say what has caused these differences as the methodology is quite similar, TEVC and the *Xenopus leavis* oocyte expression system was used in all 3 studies (including this study) it may have been possible to suggest a species-specific effect of NMDARs but the greatest difference in potency lies between the two rat clone studies.

The concentration-dependent property also expands to the onset as lower concentrations have higher τ, 0.003 µg/ml has an τ of 1072.12 ms and 3 µg/ml has a τ of 487.64 ms. The τ differences between membrane potentials are only slight and are not larger enough to suggest it is caused by voltage-dependence

4.2.1 Comparing HAE and memantine

Comparing HAE to memantine will provide some insight into whether HAE has any potential as a treatment for AD. The highest concentration of memantine achieved near complete inhibition of the agonist response, but the highest concentration of HAE only achieved modest inhibition (figure 3.2.1 and 3.3.1) This might be due to the highest concentration of HAE (3 µg/ml) when converted to M is 1.06×10^{-5} M this value is approximately 10-fold less than the highest concentration of memantine (10^{-4} M). This difference in concentration might be the reason why memantine displays higher inhibition in this study, it is also possible that there is a form of positive allosteric modulation increasing the P_{OPEN} of the GluN1A-GluN2A receptor. HAE is not 100% harmonine, so it is possible that other alkaloids or molecules can interact allosterically with the GluN1A-GluN2A receptor affecting HAE inhibition via positive allosteric modulation or an imbalanced combination of both positive and negative modulation.

It has been observed in this study that HAE is more potent than memantine at the membrane potentials -50 and -75 mV (table 4.2.1.1). This means that harmonine has therapeutic potential in AD, but that conclusion can only be made based on the IC_{50} values of this study. Kiran, 2022 found that HAE is less potent than memantine at membrane potentials of -50, -75 and -100 mV. Patel, 2018 observed an HAE IC_{50} of 0.179 µg/ml which is 0.33 µM but he did not test memantine in his study, so it is difficult to make a comparison.

The onset (τ) is slower in harmonine when compared to memantine. The highest concentration of harmonine (3µg/ml) when converted to M is ~10^{-5} M and has a τ of 487.64 ms at a membrane potential of – 50 mV, whereas memantine (10^{-5} M) has a τ of 364.10 ms are the same membrane potential.

Table 4.2.1.1: Comparison of Memantine and HAE IC_{50}. The units of concentration for HAE (µg/ml) were converted to µM to make a viable comparison to memantine (Patel, 2018; Kiran, 2022).

	IC_{50} (µM)		
V_H (mV)	-50	-75	-100
Memantine	4.02	1.48	0.828
HAE			
Current study	1.41	1.16	1.13
Patel, 2018	-	0.33	-
Kiran, 2022 HAE analogue ACB-6-90	9.38 7.695	3.93 2.969	6.09 -

4.3 Harmonine analogue (ACB-6-90) inhibition on GluN1A-GluN2A receptors expressed in *Xenopus laevis* oocytes

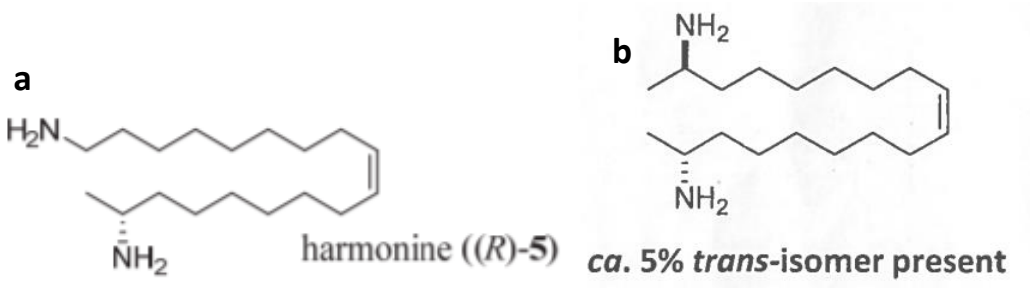

Figure 4.3.1: Harmonine analogues. (a) Harmonine. (b) ACB-6-90. A side-by-side comparison of the two molecules

ACB-6-90 is an analogue of harmonine where the amine group has been moved from the first carbon in the chain to the second carbon. ACB-6-90 similar to harmonine inhibits GluN1A-GluN2A receptors in a concentration-dependent manner (figures 3.4.1, 3.4.2 and 3.4.3). The lowest concentration of ACB-6-90 (10^{-8} M) provides minimal inhibition while the highest concentration (10^{-4} M) almost completely inhibits the agonist response. ACB-6-90 has an IC_{50} of 7.965 µM at a holding potential of -50 mV and an IC_{50} of 2.969 µM at a holding potential of -75 mV. ACB-6-90 compared to harmonine at a membrane potential of -50 has a ~five-fold difference and at -75 mV has a ~2-fold difference in potency. Harmonie and ACB-6-90 at the membrane potentials -50 and -75 mV have a IC_{50} of 1.41 µM (-50 mV), 1.16 µM (-75 mV), 7.695 µM (-50 mV) and 2.969 µM (-75 mV) respectively. This suggests that the relocation of the amine group has decreased the ability of harmonine to bind to the GluN1A-GluN2A pore.

There are no significant results to assess the voltage-dependent behaviour of ACB-6-90, the potency did increase as the membrane became more negative (7.695 µM (-50 mV) and 2.969 µM (-75 mV)). Using a non-linear regression curve fit a delta value of 0.4875 was calculated but a p-value was not calculated so these results are not applicable despite the suggested voltage dependence (figure 3.4.4).

Seemingly onset (τ) was also affected by the relocation of the amine group as there is an increase in τ of ACB-6-90 compared to the τ of harmonine. ACB-6-90 has a concentration-dependent effect on τ where 10^{-6} M has a τ of 829.1 at a membrane potential of -50 mV and at the same potential but a concentration of 10^{-4} M has a τ of 563.43. This concentration-dependent τ is seen in harmonine but harmonine has a faster decay at all comparable membrane potentials (-50 mV) and concentrations (0.3 µg/ml and 3 µg/ml). The M concentration of harmonine 0.3 and 3 µg/ml is ~10^{-6} and ~10^{-5} M respectively and

demonstrates lower τ. Harmonine at ~10^{-6} M has a τ of 631.5 ms compared to ACB-6-90 with a τ of 829.1 ms, and harmonine at a concentration ~10^{-5} M has a τ of 487.64 ms compared to ACB-6-90 with a τ of 675.63 ms.

4.4 limitations

Not every property of each substance tested was analysed e.g., an IC_{50} at a membrane potential of -25 mV was not calculated with memantine and ACB-6-90 but was for harmonine. This was due to insufficient sample sizes and not having enough viable data this also affected calculations, as larger sample sizes would create more reliable results. The expression of NMDARs in *Xenopus laevis* oocytes was not consistent in this study which in turn did affect the sample size. This also affected my ability to test more harmonine analogues as I was provided 5 other analogues.

4.5 Future work

Some of the variables I would recommend for future work is to test HAE and harmonine analogues, to increase the concentration range of HAE from 0.003 µg/ml – 3 µg/ml to 0.003 µg/ml – 30 µg/ml to allow for a comparison between memantine and ACB-6-90 at a 10^{-4} M concentration. The possibility of testing more harmonine analogues should also be explored to investigate which features affect its kinetics with NMDAR receptors, this would provide information on what changes in functional groups and molecular weight has on inhibition. Patel, 2018 found that HAE inhibits mammalian nACHRs in an open channel blocker manner, so investigation into harmonines and their analogues' effect on nACHR, would provide information on whether harmonine could be a multi-ligand target for AD treatment.

4.6 Conclusion

Based on the results of this study Harmonine has therapeutic potential, as it is more potent than memantine at -75 mV which is the approximate resting potential. It may also be a possibility that HAE possesses other molecules that have an allosteric effect on GluN1A-GluN2A receptors as voltage did not have a significant effect on potency when membrane potentials were more negative than -50 mV. This study has also shown that relocation of the amine group can potency and binding to the channel pore.

This research is a stepping stone for harmonine and puts forth an argument for its continued research as a potential therapeutic treatment for AD.

References

Alzheimer's Association (2019). *Dementia vs. Alzheimer's Disease: What Is the Difference?* [online] Alzheimer's Disease and Dementia. Available at: https://www.alz.org/alzheimers-dementia/difference-between-dementia-and-alzheimer-s.

Andreescu, C.E., Prestori, F., Brandalise, F., D'Errico, A., De Jeu, M.T.G., Rossi, P., Botta, L., Kohr, G., Perin, P., D'Angelo, E. and De Zeeuw, C.I. (2011). NR2A subunit of the N-methyl d-aspartate receptors are required for potentiation at the mossy fiber to granule cell synapse and vestibulo-cerebellar motor learning. *Neuroscience*, 176, pp.274–283. doi:10.1016/j.neuroscience.2010.12.024.

Armstrong, N., Sun, Y., Chen, G.-Q. and Gouaux, E. (1998). Structure of a glutamate-receptor ligand-binding core in complex with kainate. *Nature*, [online] 395(6705), pp.913–917. doi:10.1038/27692.

Bi, X., Gall, C.M., Zhou, J. and Lynch, G. (2002). Uptake and pathogenic effects of amyloid beta peptide 1–42 are enhanced by integrin antagonists and blocked by NMDA receptor antagonists. *Neuroscience*, 112(4), pp.827–840. doi:10.1016/s0306-4522(02)00132-x.

Blanpied, T.A., Boeckman, F.A., Aizenman, E. and Johnson, J.W. (1997). Trapping Channel Block of NMDA-Activated Responses By Amantadine and Memantine. *Journal of Neurophysiology*, 77(1), pp.309–323. doi:10.1152/jn.1997.77.1.309.

Burnashev, N., Schoepfer, R., Monyer, H., Ruppersberg, J.P., Günther, W., Seeburg, P.H. and Sakmann, B. (1992). Control by Asparagine Residues of Calcium Permeability and Magnesium Blockade in the NMDA Receptor. *Science*, 257(5075), pp.1415–1419. doi:10.1126/science.1382314.

Choi, Y.-B. and Lipton, S.A. (1999). Identification and Mechanism of Action of Two Histidine Residues Underlying High-Affinity Zn2+ Inhibition of the NMDA Receptor. *Neuron*, 23(1), pp.171–180. doi:10.1016/s0896-6273(00)80763-1.

Collingridge, G.L. and Bliss, T.V.P. (1987). NMDA receptors - their role in long-term potentiation. *Trends in Neurosciences*, 10(7), pp.288–293. doi:10.1016/0166-2236(87)90175-5.

Dai, J. and Zhou, H.-X. (2013). An NMDA Receptor Gating Mechanism Developed from MD Simulations Reveals Molecular Details Underlying Subunit-Specific Contributions. *Biophysical Journal*, 104(10), pp.2170–2181. doi:10.1016/j.bpj.2013.04.013.

Daloze, D., Braekman, J.-C. and Pasteels, J.M. (1994). Ladybird defence alkaloids: Structural, chemotaxonomic and biosynthetic aspects (Col.: Coccinellidae). *Chemoecology*, 5-6(3-4), pp.173–183. doi:10.1007/bf01240602.

Dashniani, M.G., Chighladze, M.R., Solomonia, R.O., Burjanadze, M.A., Kandashvili, M., Chkhikvishvili, N.C., Beselia, G.V. and Kruashvili, L.B. (2020). Memantine treatment prevents okadaic acid induced neurotoxicity at the systemic and molecular levels. *NeuroReport*, 31(4), pp.281–286. doi:10.1097/wnr.0000000000001375.

Esmenjaud, J., Stroebel, D., Chan, K., Grand, T., David, M., Wollmuth, L.P., Taly, A. and Paoletti, P. (2018). An inter-dimer allosteric switch controls NMDA receptor activity. *The EMBO Journal*, 38(2). doi:10.15252/embj.201899894.

Fayyazuddin, A., Villarroel, A., Le Goff, A., Lerma, J. and Neyton, J. (2000). Four Residues of the Extracellular N-Terminal Domain of the NR2A Subunit Control High-Affinity Zn2+ Binding to NMDA Receptors. *Neuron*, 25(3), pp.683–694. doi:10.1016/s0896-6273(00)81070-3.

Fernández-Tomé, P., Brera, B., ArévaloM.-A. and CeballosM.L. (2004). β-Amyloid25-35 inhibits glutamate uptake in cultured neurons and astrocytes: modulation of uptake as a survival mechanism. *Neurobiology of Disease*, 15(3), pp.580–589. doi:10.1016/j.nbd.2003.12.006.

Giacobini, E. (2004). Cholinesterase inhibitors: new roles and therapeutic alternatives. *Pharmacological Research*, 50(4), pp.433–440. doi:10.1016/j.phrs.2003.11.017.

Gielen, M., Le Goff, A., Stroebel, D., Johnson, J.W., Neyton, J. and Paoletti, P. (2008). Structural Rearrangements of NR1/NR2A NMDA Receptors during Allosteric Inhibition. *Neuron*, 57(1), pp.80–93. doi:10.1016/j.neuron.2007.11.021.

Gielen, M., Retchless, B.S., Mony, L., Johnson, J.W. and Paoletti, P. (2009). Mechanism of differential control of NMDA receptor activity by NR2 subunits. *Nature*, 459(7247), pp.703–707. doi:10.1038/nature07993.

Gilling, K.E., Jatzke, C., Hechenberger, M. and Parsons, C.G. (2009). Potency, voltage-dependency, agonist concentration-dependency, blocking kinetics and partial untrapping of the uncompetitive N-methyl-d-aspartate (NMDA) channel blocker memantine at human NMDA (GluN1/GluN2A) receptors. *Neuropharmacology*, 56(5), pp.866–875. doi:10.1016/j.neuropharm.2009.01.012.

Glasgow, N.G., Povysheva, N.V., Azofeifa, A.M. and Johnson, J.W. (2017). Memantine and Ketamine Differentially Alter NMDA Receptor Desensitization. *The Journal of Neuroscience*, 37(40), pp.9686–9704. doi:10.1523/jneurosci.1173-17.2017.

Glasgow, N.G., Siegler Retchless, B. and Johnson, J.W. (2014). Molecular bases of NMDA receptor subtype-dependent properties. *The Journal of Physiology*, 593(1), pp.83–95. doi:10.1113/jphysiol.2014.273763.

Groc, L., Heine, M., Cousins, S.L., Stephenson, F.A., Lounis, B., Cognet, L. and Choquet, D. (2006). NMDA receptor surface mobility depends on NR2A-2B subunits. *Proceedings of the National Academy of Sciences*, 103(49), pp.18769–18774. doi:10.1073/pnas.0605238103.

Heinrich, M., Mah, J. and Amirkia, V. (2021) “Alkaloids Used as Medicines: Structural Phytochemistry Meets Biodiversity—An Update and Forward Look,” *Molecules*, 26(7), p. 1836. Available at: https://doi.org/10.3390/molecules26071836.

Hogan-Cann, Adam.D. and Anderson, C.M. (2016). Physiological Roles of Non-Neuronal NMDA Receptors. *Trends in Pharmacological Sciences*, [online] 37(9), pp.750–767. doi:10.1016/j.tips.2016.05.012.

Kalbaugh, T.L., VanDongen, H.M.A. and VanDongen, A.M.J. (2004). Ligand-Binding Residues Integrate Affinity and Efficacy in the NMDA Receptor. *Molecular Pharmacology*, 66(2), pp.209–219. doi:10.1124/mol.66.2.209.

Karakas, E. and Furukawa, H. (2014). Crystal structure of a heterotetrameric NMDA receptor ion channel. *Science*, 344(6187), pp.992–997. doi:10.1126/science.1251915.

Kaur, K. (2022). *The effect of memantine and the ladybird alkaloid, harmonine, on NMDA receptor function and Alzheimer's disease*. MRes Thesis.

Kellershohn, J. *et al.* (2019) "Insects in anthelminthics research: Lady beetle-derived harmonine affects survival, reproduction and stem cell proliferation of Schistosoma mansoni," *PLOS Neglected Tropical Diseases*, 13(3), p. e0007240. Available at: https://doi.org/10.1371/journal.pntd.0007240.

Kotermanski, S.E., Wood, J.T. and Johnson, J.W. (2009). Memantine binding to a superficial site on NMDA receptors contributes to partial trapping. *The Journal of Physiology*, 587(19), pp.4589–4604. doi:10.1113/jphysiol.2009.176297.

Lane, R.M., Potkin, S.G. and Enz, A. (2005). Targeting acetylcholinesterase and butyrylcholinesterase in dementia. *The International Journal of Neuropsychopharmacology*, 9(01), p.101. doi:10.1017/s1461145705005833.

Lee, C.-H., Lü, W., Michel, J.C., Goehring, A., Du, J., Song, X. and Gouaux, E. (2014). NMDA receptor structures reveal subunit arrangement and pore architecture. *Nature*, 511(7508), pp.191–197. doi:10.1038/nature13548.

Lee, R.H.-C. *et al.* (2012) "Memantine Inhibits α3β2-nAChRs-Mediated Nitrergic Neurogenic Vasodilation in Porcine Basilar Arteries," *PLoS ONE*. Edited by A.Y.W. Chang, 7(7), p. e40326. Available at: https://doi.org/10.1371/journal.pone.0040326.

Le Bail, M. *et al.* (2014) “Identity of the NMDA receptor coagonist is synapse specific and developmentally regulated in the hippocampus,” *Proceedings of the National Academy of Sciences*, 112(2). Available at: https://doi.org/10.1073/pnas.1416668112.

Liu, J., Chang, L., Song, Y., Li, H. and Wu, Y. (2019a). The Role of NMDA Receptors in Alzheimer’s Disease. *Frontiers in Neuroscience*, [online] 13. doi:10.3389/fnins.2019.00043.

Liu, P.-P., Xie, Y., Meng, X.-Y. and Kang, J.-S. (2019b). History and progress of hypotheses and clinical trials for Alzheimer’s disease. *Signal Transduction and Targeted Therapy*, [online] 4(1). doi:10.1038/s41392-019-0063-8.

Lynch, G., Larson, J., Kelso, S., Barrionuevo, G. and Schottler, F. (1983). Intracellular injections of EGTA block induction of hippocampal long-term potentiation. *Nature*, 305(5936), pp.719–721. doi:10.1038/305719a0.

LYNCH, M.A. (2004). Long-Term Potentiation and Memory. *Physiological Reviews*, 84(1), pp.87–136. doi:10.1152/physrev.00014.2003.

Marotta, G., Basagni, F., Rosini, M. and Minarini, A. (2020). Memantine Derivatives as Multitarget Agents in Alzheimer’s Disease. *Molecules*, 25(17), p.4005. doi:10.3390/molecules25174005.

Masters, C.L., Bateman, R., Blennow, K., Rowe, C.C., Sperling, R.A. and Cummings, J.L. (2015). Alzheimer’s disease. *Nature Reviews Disease Primers*, 1, p.15056. doi:10.1038/nrdp.2015.56.

Mayer, M.L., Westbrook, G.L. and Guthrie, P.B. (1984) “Voltage-dependent block by Mg2+ of NMDA responses in spinal cord neurones,” *Nature*, 309(5965), pp. 261–263. Available at: https://doi.org/10.1038/309261a0.

McClymont, D.W., Harris, J. and Mellor, I.R. (2012). Open-channel blockade is less effective on GluN3B than GluN3A subunit-containing NMDA receptors. *European Journal of Pharmacology*, 686(1-3), pp.22–31. doi:10.1016/j.ejphar.2012.04.036.

Mony, L., Zhu, S., Carvalho, S. and Paoletti, P. (2011). Molecular basis of positive allosteric modulation of GluN2B NMDA receptors by polyamines. *The EMBO Journal*, 30(15), pp.3134–3146. doi:10.1038/emboj.2011.203.

Mota, S.I., Ferreira, I.L. and Rego, A.C. (2014). Dysfunctional synapse in Alzheimer's disease – A focus on NMDA receptors. *Neuropharmacology*, [online] 76, pp.16–26. doi:10.1016/j.neuropharm.2013.08.013.

Nagel, N. (2016). *Synthesis and Bioactivity Studies of Harmonine – the Defense Alkaloid of the Asian Lady Beetle Harmonia axyridis*. [MSc Thesis] Available at: Friedrich-Schiller-Universität [Accessed 5 Jun. 2021].

Newpher, T.M. and Ehlers, M.D. (2008). Glutamate Receptor Dynamics in Dendritic Microdomains. *Neuron*, 58(4), pp.472–497. doi:10.1016/j.neuron.2008.04.030.

Paoletti, P., Ascher, P. and Neyton, J. (1997). High-Affinity Zinc Inhibition of NMDA NR1–NR2A Receptors. *The Journal of Neuroscience*, 17(15), pp.5711–5725. doi:10.1523/jneurosci.17-15-05711.1997.

Papouin, T., Ladépêche, L., Ruel, J., Sacchi, S., Labasque, M., Hanini, M., Groc, L., Pollegioni, L., Mothet, J.-P. and Oliet, S.H.R. (2012). Synaptic and Extrasynaptic NMDA Receptors Are Gated by Different Endogenous Coagonists. *Cell*, [online] 150(3), pp.633–646. doi:10.1016/j.cell.2012.06.029.

Park, H., Popescu, A. and Poo, M. (2014). Essential Role of Presynaptic NMDA Receptors in Activity-Dependent BDNF Secretion and Corticostriatal LTP. *Neuron*, 84(5), pp.1009–1022. doi:10.1016/j.neuron.2014.10.045.

Patel, R. (2018). *Investigating the pharmacology of ladybird alkaloids on ligand-gated ion channels*. PhD Thesis.

Peatey, C.L. *et al.* (2012) "Anti-malarial drugs: how effective are they against Plasmodium falciparum gametocytes?," *Malaria Journal*, 11(1). Available at: https://doi.org/10.1186/1475-2875-11-34.

Qiu, C., Kivipelto, M. and Strauss, E.V. (2009). Epidemiology of Alzheimer's disease: occurrence, determinants, and strategies toward intervention. *Alzheimer's Disease and Mild Cognitive Impairment*, 11(2), pp.111–128. doi:10.31887/dcns.2009.11.2/cqiu.

Rammes, G., Danysz, W. and Parsons, C.G. (2008). Pharmacodynamics of Memantine: An Update. *Current Neuropharmacology*, [online] 6(1), pp.55–78. doi:10.2174/157015908783769671.

Regan, M.C., Romero-Hernandez, A. and Furukawa, H. (2015). A structural biology perspective on NMDA receptor pharmacology and function. *Current Opinion in Structural Biology*, 33, pp.68–75. doi:10.1016/j.sbi.2015.07.012.

Retchless, B.S., Gao, W. and Johnson, J.W. (2012). A single GluN2 subunit residue controls NMDA receptor channel properties via intersubunit interaction. *Nature neuroscience*, [online] 15(3), pp.406-S2. doi:10.1038/nn.3025.

Röhrich, C.R., Ngwa, C.J., Wiesner, J., Schmidtberg, H., Degenkolb, T., Kollewe, C., Fischer, R., Pradel, G. and Vilcinskas, A. (2011). Harmonine, a defence compound from the harlequin ladybird, inhibits mycobacterial growth and demonstrates multi-stage antimalarial activity. *Biology Letters*, 8(2), pp.308–311. doi:10.1098/rsbl.2011.0760.

Seago, A.E., Giorgi, J.A., Li, J. and Ślipiński, A. (2011). Phylogeny, classification and evolution of ladybird beetles (Coleoptera: Coccinellidae) based on simultaneous analysis of molecular and morphological data. *Molecular Phylogenetics and Evolution*, [online] 60(1), pp.137–151. doi:10.1016/j.ympev.2011.03.015.

Sheng, M. and Lee, S.H. (2000). Growth of the NMDA receptor industrial complex. *Nature Neuroscience*, 3(7), pp.633–635. doi:10.1038/76576.

Shields, V.D.C., Smith, K.P., Arnold, N.S., Gordon, I.M., Shaw, T.E. and Waranch, D. (2008). The effect of varying alkaloid concentrations on the feeding behavior of gypsy moth larvae, Lymantria dispar (L.) (Lepidoptera: Lymantriidae). *Arthropod-Plant Interactions*, 2(2), pp.101–107. doi:10.1007/s11829-008-9035-6.

Srivastava, S. and Srivastava, A. (2013) “Biotechnology and Genetic Engineering for Alkaloid Production,” *Springer Berlin Heidelberg eBooks*, pp. 213–250. Available at: https://doi.org/10.1007/978-3-642-22144-6_95.

Tajima, N., Karakas, E., Grant, T., Simorowski, N., Diaz-Avalos, R., Grigorieff, N. and Furukawa, H. (2016). Activation of NMDA receptors and the mechanism of inhibition by ifenprodil. *Nature*, [online] 534(7605), pp.63–68. doi:10.1038/nature17679.

Traynelis, S.F., Wollmuth, L.P., McBain, C.J., Menniti, F.S., Vance, K.M., Ogden, K.K., Hansen, K.B., Yuan, H., Myers, S.J. and Dingledine, R. (2010). Glutamate Receptor Ion Channels: Structure, Regulation, and Function. *Pharmacological Reviews*, 62(3), pp.405–496. doi:10.1124/pr.109.002451.

Twomey, E.C. and Sobolevsky, A.I. (2017). Structural Mechanisms of Gating in Ionotropic Glutamate Receptors. *Biochemistry*, 57(3), pp.267–276. doi:10.1021/acs.biochem.7b00891.

Van Marum, R.J. (2009). Update on the use of memantine in Alzheimer’s disease. *Neuropsychiatric disease and treatment*, [online] 5, pp.237–47. doi:10.2147/ndt.s4048.

Vance, K.M., Hansen, K.B. and Traynelis, S.F. (2012). GluN1 splice variant control of GluN1/GluN2D NMDA receptors. *The Journal of Physiology*, 590(16), pp.3857–3875. doi:10.1113/jphysiol.2012.234062.

Vu, H. *et al.* (2013) “Plasmodium Gametocyte Inhibition Identified from a Natural-Product-Based Fragment Library,” *ACS Chemical Biology*, 8(12), pp. 2654–2659. Available at: https://doi.org/10.1021/cb400582b.

Wang, R. and Reddy, P.H. (2017). Role of Glutamate and NMDA Receptors in Alzheimer’s Disease. *Journal of Alzheimer’s Disease*, [online] 57(4), pp.1041–1048. doi:10.3233/jad-160763.

Wollmuth, L.P. and Sobolevsky, A.I. (2004). Structure and gating of the glutamate receptor ion channel. *Trends in Neurosciences*, 27(6), pp.321–328. doi:10.1016/j.tins.2004.04.005.

Woodhull, A.M. (1973). Ionic Blockage of Sodium Channels in Nerve. *Journal of General Physiology*, 61(6), pp.687–708. doi:10.1085/jgp.61.6.687.

Yao, Y., Belcher, J., Berger, Anthony J., Mayer, Mark L. and Lau, Albert Y. (2013). Conformational Analysis of NMDA Receptor GluN1, GluN2, and GluN3 Ligand-Binding Domains Reveals Subtype-Specific Characteristics. *Structure*, 21(10), pp.1788–1799. doi:10.1016/j.str.2013.07.011.

Yong, E. (2013). Invasive ladybird has biological weapon. *Nature*. doi:10.1038/nature.2013.13011.

Yuan, H., Hansen, K.B., Vance, K.M., Ogden, K.K. and Traynelis, S.F. (2009). Control of NMDA Receptor Function by the NR2 Subunit Amino-Terminal Domain. *Journal of Neuroscience*, 29(39), pp.12045–12058. doi:10.1523/jneurosci.1365-09.2009.